NASA CR-54208

DEVELOPMENT OF A HIGH TEMPERATURE BATTERY

by

W.J. Subcasky, D.N. Stamires, and A. Parker-Jones

prepared for

NATIONAL AERONAUTICS AND SPACE ADMINISTRATION

CONTRACT NAS3-6002

AERONUTRONIC
DIVISION OF PHILCO CORPORATION
A SUBSIDIARY OF Ford Motor Company
FORD ROAD / NEWPORT BEACH, CALIFORNIA

Request for copies of this report should be referred to:

National Aeronautics and Space Administration
Office of Scientific and Technical Information
Washington, D. C. 20025
Attention: AFSS-A

NASA CR-54208
Aeronutronic Publication No. U-2844
W. O. 2261

FIRST QUARTERLY TECHNICAL REPORT

DEVELOPMENT OF A HIGH TEMPERATURE BATTERY

by

W. J. Subcasky, O. N. Stamires, and A. Parker - Jones

prepared for

NATIONAL AERONAUTICS AND SPACE ADMINISTRATION

October 20, 1964

Technical Management
NASA Lewis Research Center
Cleveland, Ohio
Space Power Systems Division
Meyer R. Unger

APPLIED RESEARCH LABORATORY
Aeronutronic Division
Philco Corporation
Newport Beach, California

OBJECTIVE

The objective of this program is to develop a high energy density battery capable of operation for three days at 800°F (424°C) in an environment approximately the same as exists on the planet Venus. The battery should also be capable of activation within less than ten minutes after exposure to 800°F temperature. The battery will be able to supply power to an instrument package in the Venus environment.

A thin synthetic zeolite membrane will be used to separate the anode and cathode section of the battery. The zeolite, acting as a solid electrolyte permeable only to cations, will eliminate many of the problems associated with the solubility and reactivity of materials in high temperature battery systems. The zeolite membrane will permit the use of high energy density components to produce a light weight battery.

SUMMARY

11040

The literature survey indicates that the crystalline, synthetic zeolites are the most suitable solid electrolytes for a battery designed to operate for three days at a temperature of 425°C. The resistances of the glasses and the oxide deficient materials are too high at these temperatures. Although the noncrystalline porcelains have lower resistances, they do not appear to undergo ion exchange with divalent cations. This restricts the design of the battery since molten salts containing monovalent cations must be in contact with the porcelains if electrolytic conductivity is to occur.

The crystalline zeolites are electrolytic conductors with a low resistivity. Rapid and, in some cases, complete ion exchange has been achieved between the zeolites and both mono- and divalent cations. The zeolites have been used as solid electrolytes in low temperature fuel cells and batteries. Thin membrane can be obtained by vacuum hot pressing or by bonding with a ZrO_2-H_3PO_4 mixture.

Calculated and experimentally determined potentials for possible anode and cathode couples both as pure molten salts and as solutions in molten LiCl-KCl eutectic are tabulated. Electrochemical characteristics of molten $BiCl_3$, $FeCl_3$, CuCl, $CuCl_2$, AgCl, and $K_2Cr_2O_7$ and of K_2CrO_4 in LiCl-KCl eutectic are presented.

Equipment to vacuum hot press zeolite membranes and to measure their resistance as a function of temperature and surrounding atmosphere is described. Preliminary studies on the ion exchange properities and x-ray diffraction patterns of zeolites with Ag^+ and Cu^{++} are discussed. Resistivities for a zeolite membrane as a function of temperature have been measured.

Author

CONTENTS

ILLUSTRATIONS

TABLES

SECTION 1

LITERATURE SURVEY

During this portion of the program, the literature survey was directed towards the areas of immediate importance; namely anodes, cathode, and solid electrolyte with particular emphasis upon the synthetic crystalline zeolites.

1.1 ANODES

The alkali and alkaline earth metals are generally used as anodes in thermal cells. The equivalent weight of the most important anode materials, their approximate potentials as measured versus a Pt/Pt(II) reference in actual thermal cells (33), and their melting points are shown in Table I.

The potential given for calcium is undoubtedly that of the calcium-lithium alloy which invariably forms when metallic calcium is brought in contact with Li^+- containing molten electrolytes. The alloy which is formed by the reduction of lithium ions by metallic calcium is a liquid at the operating temperature of the battery. The potential of sodium is estimated from the calculated reversible decomposition voltage of NaCl at 450°C (19). Sodium is expected to have an activity only slightly lower than calcium and hence a Li-Na alloy would probably form in the presence of Li^+.

A commercially available Li-Al alloy called LA141 has been used as an anode in thermal cells (46). This alloy contains 13-15 percent lithium and 1.0 to 1.5 percent aluminum. It reportedly gives cell voltages both on open circuit and under drain about 0.5 to 0.6 volts higher than pure magnesium. The particular advantage of this alloy is its high electrochemical activity without the formation of a liquid anode.

TABLE I

CHARACTERISTICS OF ANODE MATERIALS

Material	Potential Versus Pt-Pt(II)	Equivalent Weight	M.P. (^{o}C)
Aluminum	-1.71	8.99	659.7
Lithium	-3.34	6.94	186
Magnesium	-2.55	12.16	651
Calcium	-3.23	20.04	842
Sodium	Approx. -3.23(a)	23.0	97.5
Li-Mg Alloy	Approx. -3.10(b)	-----	600

(a) Potential calculated from Reference (19). See text.

(b) From Reference (46). See text.

1.2 CATHODES

Practical cathode systems for high temperature battery applications are almost exclusively those involving compounds between oxygen and the transition and nonmetallic elements. The cathode depolarizers are generally in the form of oxides. Examples of various oxides which have been used as cathodes in thermal batteries are CuO (36), Sb_2O_3 (36), and FeO_x (35). The oxides are used because they are only slightly soluble in the molten LiCl-KCl electrolyte generally used in thermal batteries. The oxides have the required thermal stability and many appear to be reversible (25). The slight solubility of some of the oxides would be expected to decrease the active life of a thermal battery especially in batteries designed for extended periods of operation.

It is anticipated that using an insoluble cathode depolarizer will decrease, to some extent, the energy and power densities of a thermal cell. As would be predicted by the Nernst equation, the potential of a metal-metal oxide electrode is more negative (IUPAC, Stockholm convention) than that of the corresponding metal-metal ion electrode. Table II shows this shift for a few systems in a molten LiCl-KCl eutectic. A more negative cathode would give a lower cell voltage when coupled with an anode.

It is highly possible that in a cell using a solid electrolyte as a separator, a pure molten cathode depolarizer could be used. In other words, no additional molten electrolyte is needed in the cathode compartment. The omission of the inert electrolyte would obviously increase the energy density of the cell.

TABLE II

ELECTRODE POTENTIALS AT 450°C

Couple	Pure Salt	LiCl-KCl Eutectic
Li(I)-Li	-2.773	-2.773
Ca(II)-Ca	-2.659	-2.66
Mg(II)-Mg	-1.809	-1.943
NiO-Ni	------	-0.771 (25)
Cr(III)-Cr	-0.763	------
Cr(II)-Cr	-0.657	-0.758
Cu_2O-Cu	------	-0.750 (25)
V(III)-V	-0.665 (227 0)	------
Fe(II)-Fe	-0.686	-0.535 (27)
Fe(III)-Fe	-0.405 (319 V)	------
V(III)-V(II)	------	-0.217 (27)
Cu(I)-Cu	-0.424	-0.214
Ni(II)-Ni	-0.493	-0.158
Sb(III)-Sb	-0.408 (221 V)	-0.033
Cr(III)-Cr(II)	------	-0.006
Ag(I)-Ag	0.000	0.000
Bi(III)-Bi	-0.233 (441 V)	+0.049
Cu(II)-Cu	+0.053	
PtO-Pt		+0.118 (25)
Pd(II)-Pd	+0.124	+0.421
Cr(VI)-Cr(III)		+0.545 (6)
Cu(II)-Cu(I)		+0.592
Fe(III)-Fe(II)		+0.617 (27)
Pt(II)-Pt	+0.312	+0.637
Au(I)-Au	+0.574	+0.948
Cl_2-Cl	+0.611	+0.953 (27)

References: Pure Salt (19); LiCl-KCl eutectic (26) except where noted otherwise.

Concentrations expressed as ion fractions. Value in brackets indicate temperatures at which vaporization (V) or decomposition (0) occurs. Potentials in these cases are at temperatures slightly lower than those at which the transition occurs.

Standard potentials for possible cathode depolarizers both as pure molten halides and in a LiCl-KCl eutectic at 450°C are given in Table II. Potentials of Li, Ca, and Mg are given for comparison. The reference electrode for both systems is Ag(I)-Ag and the concentration units are expressed in cationic fraction. The voltages for the pure salts (19) were calculated from thermodynamic data while those for the LiCl-KCl solution were experimentally determined. Many of these potentials have been confirmed in thermal cells using a LiCl-KCl electrolyte (33).

The standard potentials listed in Table II can be used to estimate the voltage of complete cells by the relation:

$$E_{cell} = E_{cathode} - E_{anode}$$

The unpublished work of H. A. Laitinen and his students (24) contains much information concerning the electrochemical properties of possible cathode depolarizers dissolved in LiCl-KCl eutectic. These results are summarized according to the various elements.

1.2.1 CHROMIUM

The reduction of Cr(VI), added as K_2CrO_4, is irreversible and occurs in the region of -0.2 to -0.9 volts versus 1M Ag(I).[4] The reduction product is insoluble and contains Li, Cr(VI), Cr(III), and $O^=$. The reduction of Cr(III), added as $CrCl_3$, is irreversible and occurs in the range of +0.5 to +0.1 volts. The reduction of Cr(II) occurs at -1.0 volts and is reversible.

1.2.2 COPPER

The Cu(II)-Cu(I) couple appears to be slow-potentiometrically, it does not follow the Nernst equation and voltammetrically, a mixture of Cu(II) and Cu(I) shows a discontinuity in the slope of the current-voltage curve as it crosses the zero current axis.

1.2.3 BISMUTH

A single, reversible, three-electron reduction wave at +0.12 volts versus 1m Ag(I) was observed with Bi(III).

1.2.4 IRON

Fe(III) undergoes a reversible, one-electron reduction to Fe(II) at +0.8 volts. The Fe(II) itself is reversibly reduced to Fe at -0.60 volts.

1.2.5 GOLD

Potentiometric measurements indicate that the Au(I)-Au couple is reversible with a standard potential of +0.948 volts versus 1m Ag(I).

1.3 SOLID ELECTROLYTES

There are three general types of solid electrolytes which might be considered for use in a high temperature battery. These are:

(1) Oxide deficient structures.

(2) Porcelains and ceramics.

(3) Synthetic, crystalline zeolites.

Each of these will be considered separately. However, since the proposed system uses a zeolite solid electrolyte, the major portion of the survey was directed towards this subject.

1.3.1 OXIDE DEFICIENT STRUCTURES

Oxide deficient materials of the form $(ZrO_2)_{0.85}$ $(Y_2O_3)_{0.15}$ or $(ZrO_2)_{0.85}$ $(CaO)_{0.15}$ have been used as solid electrolytes in high temperature fuel cells. The CaO system seems to form cubic crystals of the fluorite type, with all cation lattice sites occupied, but with one anion site vacant for each CaO molecule included. Transfer of oxide ions from one vacant anion site to another accounts for the conductivity of these materials. However, the temperature must be rather high (about 1000°C) before the conductivity becomes high enough for practical use as a solid electrolyte.

1.3.2 PORCELAINS AND CERAMICS

The electrolytic conductivity of glass at elevated temperatures has been known for some time. This conducitivty has been used in the preparation of sodium coulometers and reference electrodes. When used as a diaphragm between two fused salts, glass has a resistance of 2000 to 5000 ohms in the temperature range of 350 to 550°C (7).

More recently, porcelain-type materials (sodium aluminum silicates) have been used for reference electrodes (23). The porcelain used in these electrodes is prepared by fusion of various glass and clay compositions and can be used at higher temperatures than corresponding electrodes using glass. In addition, the resistivity of the porcelain is lower than that of the glass. Resistivities of some porcelain materials as a function of composition and temperature are shown in Table III. Conductivity of these porcelain materials has been shown to be solely by sodium ions and not by transfer of electrons or oxide ions. These porcelains may then be considered to be solid electrolytes where the transference number of sodium ions is unity.

TABLE III

RESISTIVITY OF PORCELAIN (23)

Temperature °C	2.5% Na_2O, 73.1%SiO_2 24.4% Al_2O_3	10% Na_2O, 54% SiO_2 36% Al_2O_3
400		730
450		420
550		140
650		64
700		42
860		25
900	430	20
940	380	
1000	300	

Ion exchange studies (22) with porcelains of this type in certain molten salts showed that with potassium, rubidium, or silver melts, exchange was complete and reversible; in lithium, cuprous, or cesium melts partial exchange occurred. No exchange was noted with melts containing NH_4^+, Mg^{++}, Ba^{++}, Zn^{++}, Pb^{++}, or Cd^{++}. The extremely small probability of two cation sites which are simultaneously vacant and sufficiently close together to accept a divalent cation was given as the reason for lack of exchange of divalent cations. A similar reason was given for the lack of electromigration of divalent cations in glass.

Porcelain membranes have been used as a barrier to prevent mixing of the liquid anolyte and catholyte of secondary molten salt cells while still maintaining electrolytic conductivity (40). Cells of the type M/MCl, NaCl/P/NaCl, AgCl/Ag where M was the anode material, MCl was its oxidized product in a chloride melt, and P was a porcelain membrane, were operated for periods as long as five or six days.

Recently a study of cells using tin alloys of sodium and lithium as anodes and various porcelains and glasses as separators has been reported (18). All of these separators had resistivities greater than 10^2 ohm-cm at a temperature of about 550°C.

High temperature cells using a porcelain electrolyte to separate two dissimilar metals have been prepared. The cells, called Austin Cells, generate electrical energy by the oxidation of one metal electrode while the other metal, usually silver, serves as an inert electrode for the reduction of oxygen. The glass or porcelain enamel separating the two metals served as the electrolyte or ionic conductor (21).

1.3.3 ZEOLITES

The natural and synthetic zeolites are aluminosilicates of the alkali or alkaline earth metals. The synthetic zeolites are usually prepared by crystallization from aluminosilicate gels. The zeolites prepared in this manner have the general composition

$$Na_x \quad (AlO_2)_x \ (SiO_2)_y$$

and consist of alumina and silica tetrahedra arranged in an orderly fashion so as to form basic cubo-octahedra units, which in turn are linked together in various types of arrangements to form the unit cell. It is these arrangements which give rise to the different types of zeolites. Thus the structure of so-called "Type A" zeolite has been found (13) to consist of twelve alternating AlO_4 and SiO_4 tetrahedra per unit cell. Each unit cell also contains twelve sodium ions in the interstices. The arrangement of the tetrahedra in the unit cell produces a large central cage, 11.4 Å in diameter, connected to six similar cages by 8-membered oxygen rings having an opening of 4.2 Å. In addition, the large cage is linked to 8 smaller cavities 6.6 Å in diameter by opening 2.0 Å in diameter. It is these well-defined passages in the zeolite lattices which gives these materials their molecular sieve properties. In the type X and Y zeolites, the large cavities are connected by channels of approximately 12 Å diameter (15). These channels for some natural zeolite types are shown in Figure 1.

The four fold coordination of Al atoms with oxygen in the zeolite lattice creates a uninegative charge on each of the (AlO_4) units. This requires the occlusion of one monovalent or a half of a divalent cation in the lattice for electrical neutrality. A small fragment of the lattice can be represented as follows:

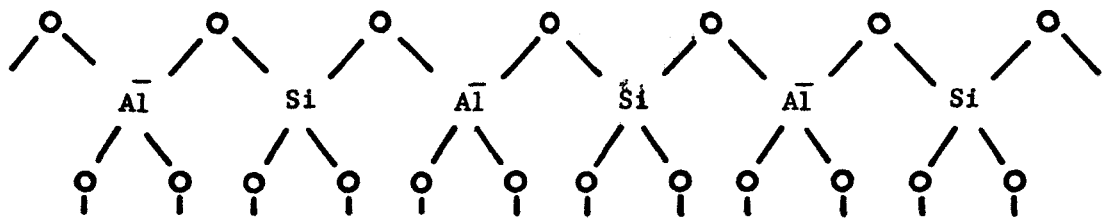

The negative lattice sites are fixed in the framework and interact with the cations, primarily through coulombic forces. This type of bonding and the open crystal framework permits easy exchange and diffusion of the cations in the lattice (16).

a. Preparation and Characterization

Synthetic zeolites are usually prepared by crystallization from aluminosilicate gels in the presence of excess alkali. The hydrous gels are prepared with various amounts of sodium silicate, sodium aluminate, and sodium hydroxide. In some cases, all or a portion of the sodium salts are replaced by the

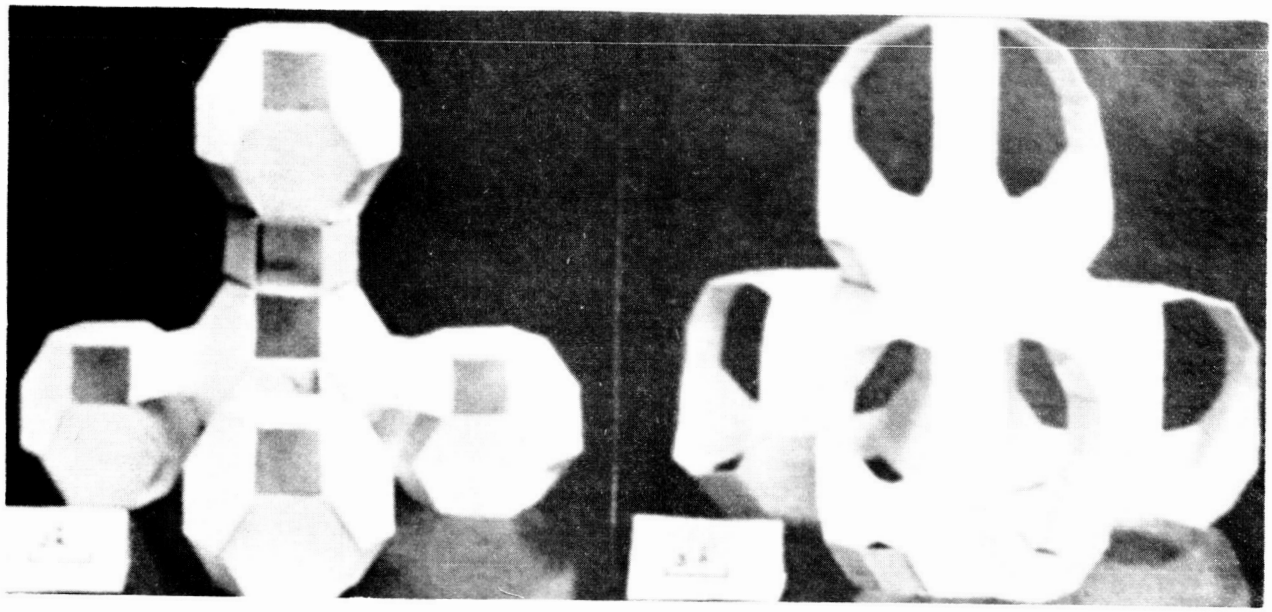

(a) (b)

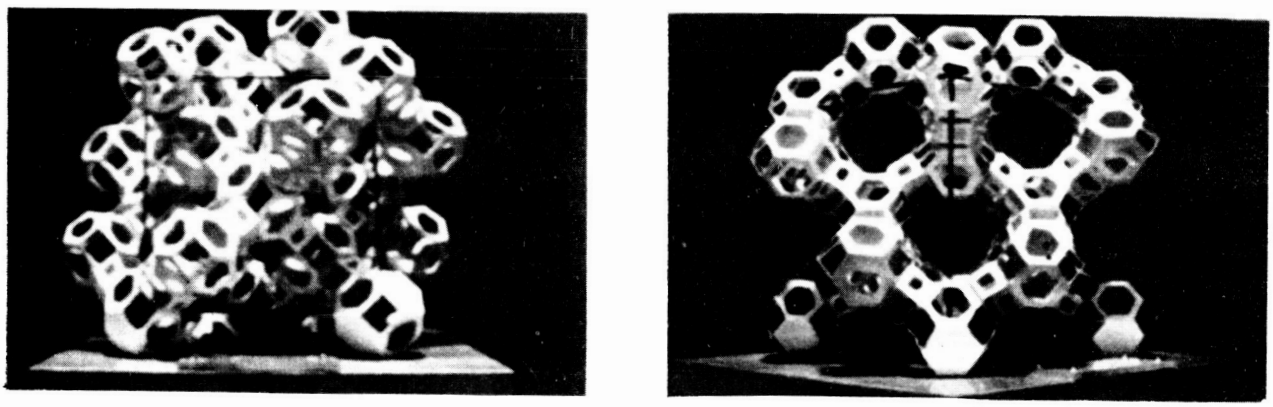

(c) (d)

(a) THE TETRAHEDRAL CO-ORDINATION OF SODALITE-TYPE CAGES.
(b) EQUIVALENT DIAMOND-LIKE STACKING OF SUPER-CAGES.
(c) PERSPECTIVE OF THE FAUJASITE ALUMINOSILICATE FRAMEWORK NORMA LTO THE (100) FACE.
(d) PERSPECTIVE OF THE FAUJASITE FRAMEWORK LOOKING IN THE 110 DIRECTION.

R05300

FIGURE 1. STRUCTURE OF ZEOLITES

corresponding potassium salts. By varying the amounts of materials used to form the gels and by varying the temperature of crystallization, various synthetic zeolites have been prepared. A list of some crystalline zeolites that have been prepared is given in Table IV. The type designation is that assigned by Union Carbide Corporation to its various types of molecular sieves. The compositions as given are those which are usually obtained. Slight variation in composition are possible without modifying the zeolite type. In fact, the zeolite type is determined not by its composition but by its x-ray diffraction pattern.

TABLE IV

SYNTHETIC ZEOLITE CHARACTERISTICS

	Composition (1)					
Type	$\frac{a}{Na_2O}$	$\frac{b}{K_2O}$	$\frac{c}{Al_2O_3}$	$\frac{d}{SiO_2}$	"d" Spacings in Order of Line Intensity (2)	Reference
A	1	0	1	2		31
B	1	0	1	3-5		14
D	0-1	1-a	1	4.7	2.94, 6.89, 9.42	8
E	0-1	1-a	1	2	9.53, 2.86, 3.00	10
F	0	1	1	2	6.95, 2.96, 3.09	29
G	0	1	1	3.6		14
H	0	1	1	2		14
J	0	1	1	1.9-2.3	2.89, 3.13, 6.86	43
L	0	1	1	5.9-6.9	15.8, 4.57, 3.91	44
M	0	1	1	2.0-2.2	3.10, 2.60, 4.25	12
Q	0	1	1	2.2	11.8, 3.01, 2.67	11
R	1	0	1	3.45-3.65	2.95, 9.51, 4.37	28
S	1	0	1	4.6-5.9	7.16, 2.97, 4.12	45
T	0.1-0.8	1-a	1	6.4-7.4	11.3, 3.72, 2.85	9
W	0	1	1	3.3-4.9	3.25, 3.17, 2.96	30
X	1	0	1	2.0-3.0	14.47, 3.81, 2.88	32
Y	1	0	1	3-5	14.4, 5.69, 3.78	42

(1) Composition of material as usually prepared.

(2) Generally the fully hydrated form as usually prepared.

The gel composition and crystallization temperature are quite critical in determining the type of zeolite which is produced. As a specific example, Type F and Type J zeolites have practically the same composition with the exception of the noncritical water content. The oxide ratio of the materials used to prepare the gel are different (Table V) and both zeolites are crystallized at 100°C. The x-ray diffraction patterns are completely different as shown in Table VI.

TABLE V

OXIDE RATIO OF GELS

	Type F	Type J
K_2O/SiO_2	1.4 - 4.0	4
SiO_2/Al_2O_3	1.0 - 3.0	4
H_2O/K_2O	10 - 20	10

TABLE VI

X-RAY POWDER DIFFRACTION DATA FOR POTASSIUM ZEOLITES

Type F		Type J	
d Spacing °A	Relative Intensity	d Spacing °A	Relative Intensity
6.95	100	6.86	54
6.51	11	4.77	32
3.48	21	4.72	16
3.09	56	4.27	15
2.96	72	4.00	51
2.81	39	3.23	46
2.25	8	3.13	93
1.74	6	3.04	40
1.69	6	3.00	41
1.64	5	2.97	36
		2.89	100
		2.87	61
		2.66	20
		2.64	25
		2.58	23

References: Type F (29)

Type J (43)

The "d" spacings for the three most intense lines of the other types of zeolites are also shown in Table IV. The "d" spacings are for the zeolites as prepared. Slight changes in relative intensities and positions of the diffraction lines are noted when the cation of the zeolite is changed. This shift is shown in Table VII for the 111 plane in Type X zeolite. Small changes in line positions are also noted with changes in the water content of the zeolite.

TABLE VII

SHIFT OF d_{111} FOR TYPE X ZEOLITE AS A FUNCTION OF EXCHANGED CATION (32)

Cation	Percent Exchanged	d_{111} ^{o}A
Na^{+}	100	14.47
Ca^{++}	89	14.37
Ag^{+}	85	14.37
Ce^{+3}	77	14.42
Li^{+}	59	14.37
NH_4^{+}	81	14.41
Ba^{++}	93	14.43

Crystallographic examination of various types of synthetic zeolites yield the following unit cell compositions (16).

Type A $Na_{12}\left[(AlO_2)_{12}\ (SiO_2)_{12}\right]$

Type Y $Na_{53}\left[(AlO_2)_{53}\ (SiO_2)_{139}\right]$

Type X $Na_{88}\left[(AlO_2)_{88}\ (SiO_2)_{104}\right]$

An extensive study of the hydrated forms of the Type 4A, 5A, and 13X has also been reported (15). This study includes X-ray diffraction and electron density observations and the application of the three-dimensional Fourier method to the refinement of atomic positions and the location of cations.

Zeolites can be obtained containing various cations. In most cases, the synthetic zeolites are first prepared in the Na^+ or K^+ form, and then the desired cation form obtained by ion exchange as described in Paragraph 1.3.3b. However, it is sometimes possible to synthesize the zeolite in the desired cation form. Zeolites containing either $(CH_3)_4N^+$, $(CH_3)_3NH^+$, or $(CH_3)_2NH_2^+$ (4-1), Ba^{++} (1), Rb^+ and Cs^+ (3), and Li^+ (4) have been prepared. A summary of these preparations have been published (2).

b. Ion Exchange Properties

As described before, the interaction between the negative lattice sites fixed in the zeolite framework and the cations is principally through coulombic forces. Because of this type of bonding between the cations and the cation sites and also because of the open crystal framework, these cations are very easily exchanged for other cations of different size and charge without much distortion of the crystal lattice.

A summary of the studies of the ion exchange properties of some of the various types of synthetic zeolites produced by Union Carbine Corporation is given in Table VIII. The numberals in Table VIII indicate the percent of the exchange which was achieved. No attempt was made to obtain complete exchange except for the studies on the Type Y zeolite. The exchange studies were performed by equilibrating a portion of the zeolite with an aqueous solution of the exchanging ion. The (+) sign indicates exchange did occur but no quantitative information on the extent of exchange was given. X-ray diffraction patterns are given for the various exchanged forms of Types A, D, L, Q, and X. In addition, exchange studies on Type X zeolite with K^+, Li^+, Ca^{++}, and Ag^+ from alcoholic solutions have been made (20). By the use of percolating techniques (16), almost complete exchange has been achieved in some cases. Thus, with Type A zeolite, the exchange with Li^+ was 98.6 percent; with K^+, 99.8 percent, and with Ag^+, 99.7 percent.

c. Conductivity

The highly mobile cations in the zeolite lattice result in an unusually high electrical conductivity for ionic crystals. It has been long recognized that this conduction mechanism is ionic in nature (34) and is due to the self-diffusion of cations in the crystal lattice (38, 16). That this proceeds with a relatively low activation energy has been attributed to the high density of the cations ($\sim 10^{22}$ monovalent cations/gram of crystal) and to weak electrostatic interaction of the cation with the cation site ($\sim$10 kilocal/mole). This low activation energy for cation diffusion is also caused by the open space available in the diffusion path.

TABLE VIII

ION EXCHANGE PROPERTIES OF SYNTHETIC ZEOLITES

Cation	Zeolite Type A	D	E	F	L	M	Q	R	W	X	Y
Li^+	33	66	47.2	+	47.6		58	+	22.6	59	
Na^+	100	95	+	+	41.4	+	65	100	69	100	100
K^+	46	+	+	100	100	100	100	+	100		97.6
Rb^+	36										61.4
Cs^+	31										77.1
NH_4^+	39			+		+				81	
Ag^+	88					+				85	
Tl^+	~ 70	72		+	39.1						78
Mg^{++}	43		51.8				45	+	52.9		71.0
Ca^{++}	72	92	89.4		+	+	81	+	52	89	95.7
Sr^{++}	+	96			48.3		64	+	62.7		74.2
Ba^{++}	+				73.2		66	+		93	95.6
Zn^{++}	+	71	82.3		22.8		64	+	89		
Cd^{++}	+										
Hg^{++}	+										
Mn^{++}	+								+		
Co^{++}	+										
Ni^{++}	+										
Ce^{+++}										77	
Reference	13 17	8	10	29	44	12	11	28	30	32	16

The ionic conductivity increases with increasing temperature and is given by (16):

$$\sigma = \frac{N\lambda^2 q^2}{h} \exp\left(-\frac{\Delta G}{RT}\right) \qquad (1)$$

where σ = conductivity

N = number of charge carriers

q = carrier charge

λ = distance between cation sites

ΔG = free energy for conduction

The effect of cation density and temperature are shown in Figure 2 for a series of zeolites in the Na^+ form. The SiO_2/Al_2O_3 ratio was varied in such a manner as to go from the Type X zeolite (2.40) to the Type Y (5.20). The ratio is also an indication of the cation density since electrical neutrality requires that every aluminum atom in the crystal be balanced with a positive charge.

Figure 3 shows the effect of the radius and the charge of the cationic carriers upon the free energy for conduction. According to Equation (1), an increase in ΔG causes a decrease in the conductivity. For monovalent cations the coulombic attraction between the cation and the cation site decreases as the size of the cation increases. For larger cations, the number capable of migration decreases because of steric hindrance. For divalent cations the conductivity decreases with increasing size because of the greater bonding to two separated negative charges with the larger, more easily polarized cations.

The effect of various adsorbed phases upon the conductivity of various synthetic zeolites have also been studied (38). It was found that the potential energy barrier for the conduction process is decreased and hence the conductivity increased by adsorbed molecules. Polar molecules (e.g., H_2O and NH_3) exhibit a strong association through ion-dipole interactions with the mobile cations. Completely hydrated zeolites at room temperatures have conductivities approaching that of aqueous solutions. These observations have been confirmed for zeolites containing phosphoric acid.

The effect of various factors upon the conductivity of crystalline zeolites can be summarized. The conductivity increases with

(1) increasing temperature.

(2) increasing cationic density.

(3) increasing cation charge.

(4) increasing cationic radius except for very large cations where steric hindrance reduces the charge carriers available for conduction.

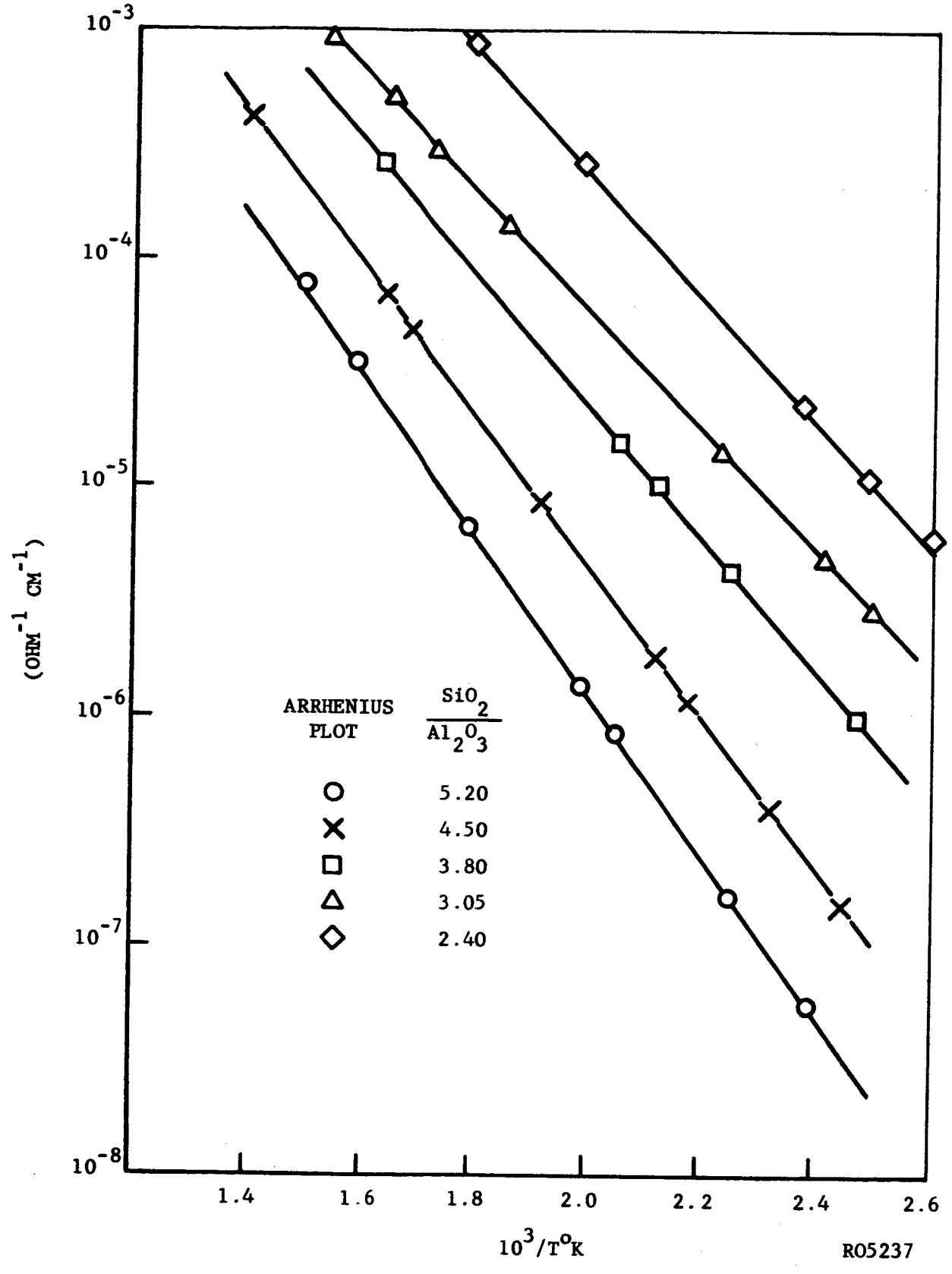

FIGURE 2. CONDUCTIVITY OF THE X-Y ZEOLITE SERIES

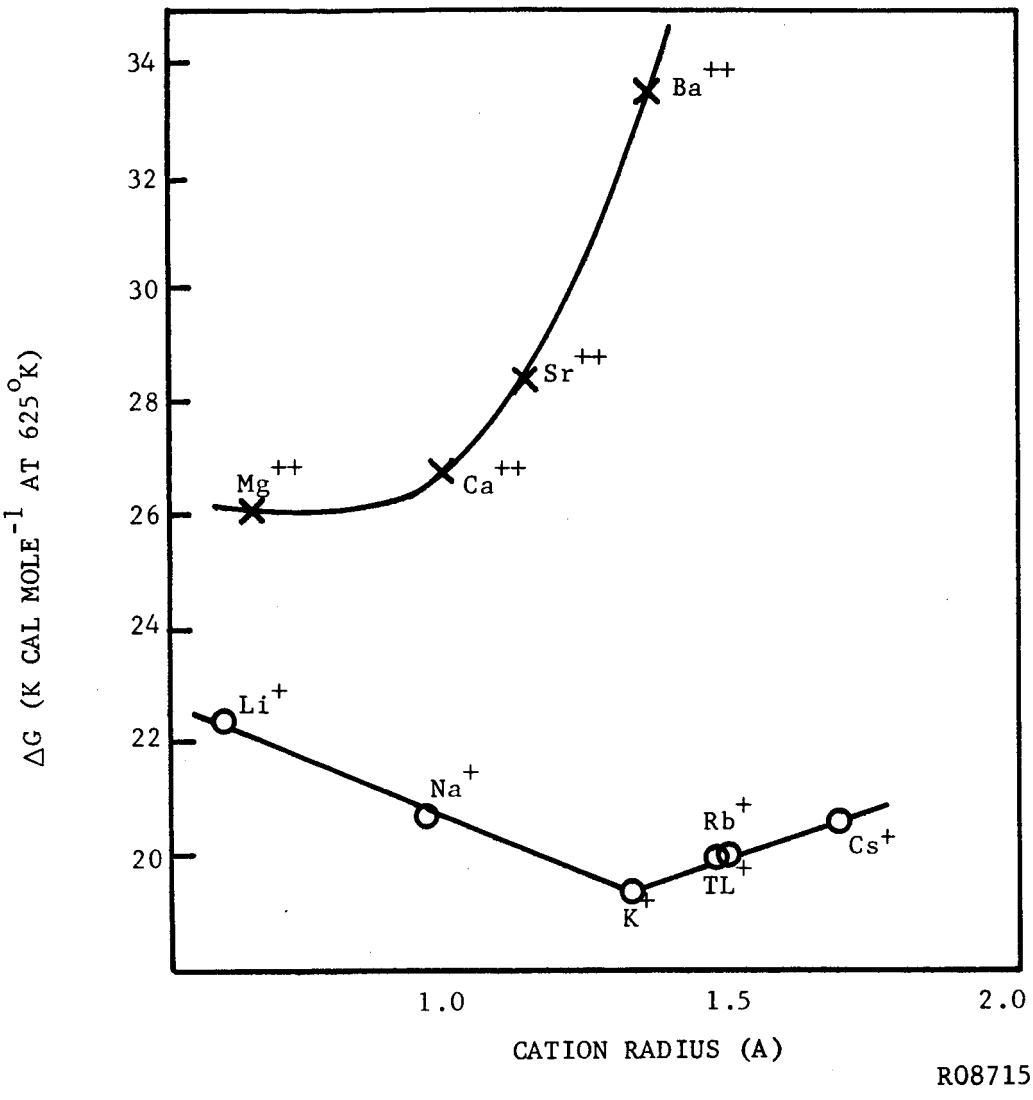

FIGURE 3. FREE ENERGY VALUES FOR MONOVALENT AND DIVALENT-CATION EXCHANGE Y ZEOLITES FROM (16).

(5) decreasing cationic radius for divalent ions.

(6) adsorption of polar molecules.

d. Applications

The principal application of the synthetic zeolites is as molecular sieves to selectively adsorbed and separate various molecules. However, for this program, the application of the ionic conductivity of the zeolite as a solid electrolyte in a high temperature battery is the prime requisite. The Astropower Laboratory of Douglas Aircraft (5) have used synthetic zeolites as solid electrolytes in ambient temperature fuel cells. In this study, the zeolites were bonded into thin wafers using ZrO_2-H_3PO_4 cements. The large amount of phosphoric acid contained in these wafers yield specific conductivities of the order of 10^{-2} to 10^{-1} ohm^{-1} cm^{-1} for high relative humidities at temperatures below 100°C.

The use of another type of inorganic ion exchange material for use as a solid electrolyte in a fuel cell should be mentioned (37). These materials were prepared from the phosphates of heavy metals such as tin, titanium, niobium, and germanium. Exchange capacities of 6 to 8 milliequivalents per gram and resistance values of the order of 1 to 10 ohm- cm^2 were obtained for water saturated membranes. These materials might be useful as solid electrolytes at higher temperatures.

SECTION 2

EXPERIMENTAL STUDIES

2.1 CATHODES

The basic purpose of this portion of the experimental study is the measurement of the potentials with current drain of selected materials that would give the most energetic cathodes.

Electrode materials tested include gold, platinum, graphite, and copper. Cathode depolarizers tested include the chlorides of copper (II), copper (I), silver (I), bismuth (III), iron (III) and the chromate and dichromate of potassium. Some of these salts were tested in solvents and in the presence of cell discharge by-products such as calcium ion. Graphite was used as the auxiliary electrode material in all experiments.

A silver wire in equilibrium with a dilute solution of silver ion in a fused LiCl-KCl eutectic was used as the reference electrode in most experiments.

2.1.1 EQUIPMENT

Figures 4 and 5 are block diagrams of the equipment used for polarization measurements on cathode materials.

a. Furnace

Hevy-Duty Electric Multiple Unit Furnace type MU-3018 - 115-230 volts - 2575 watts. Two of the four heating units were disconnected as shown in the schematic wiring diagram (Figure 5) so that only the upper half of the vertical tube type furnace was heated.

b. Controller

Bristol series 536 Free-Vane Electronic Indicating Controller. The Bristol Company, Waterbury 20, Connecticut.

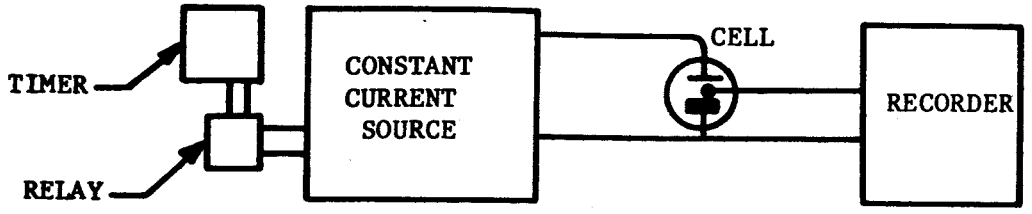

FIGURE 4. BLOCK DIAGRAM OF APPARATUS FOR POLARIZATION STUDIES

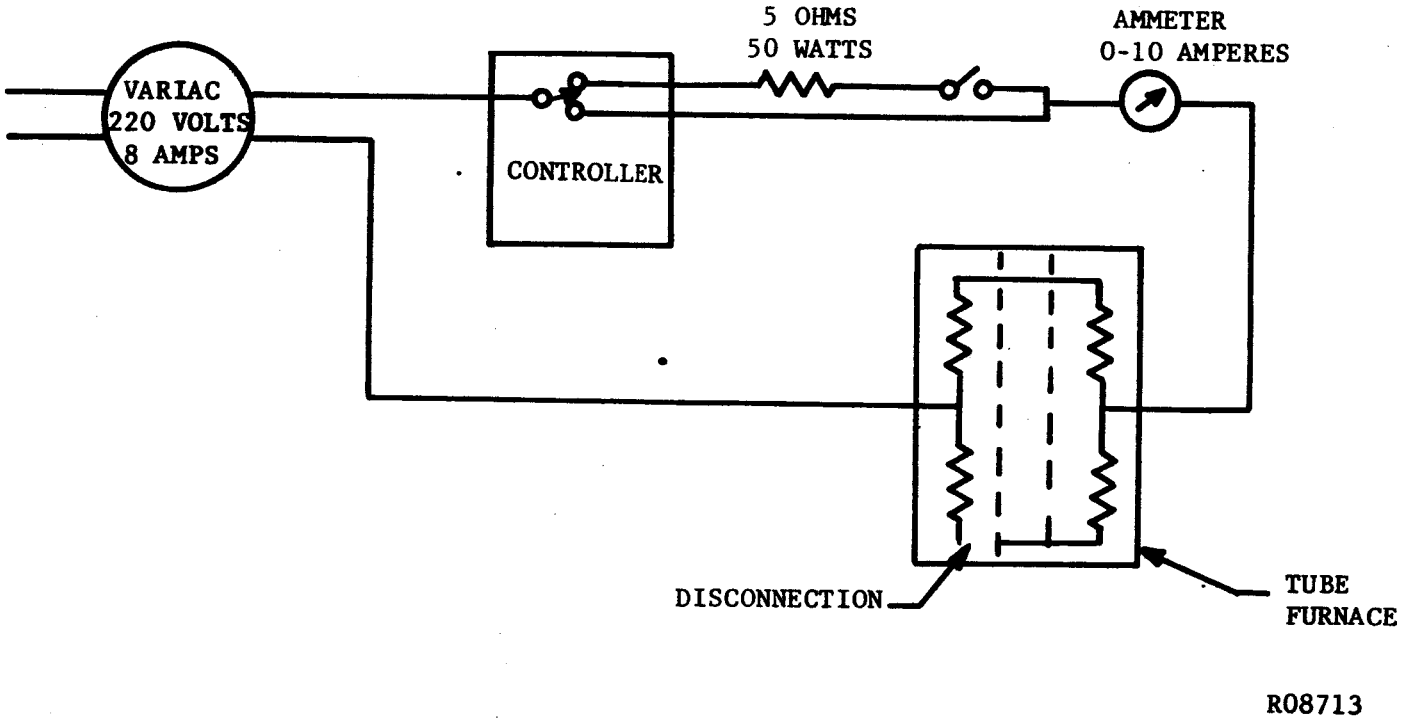

FIGURE 5. BLOCK DIAGRAM OF CELL HEATING APPARATUS

c. Recorder

Sargent Recorder Model MR, 250-mv full scale deflection. Chart speed was 0.2 inch per minute.

d. Constant Current Source

Harrison Laboratories Model 6201A. The power supply was operated in the constant current mode with an external programming resistor. The programming resistor was switched either manually or automatically with a cycling timer to change the current drains through the cell.

e. Electrolytic Cells

A schematic diagram of the first cell used in the experiments is shown in Figure 6. All of the glass parts were Pyrex. The cell container was a test tube 300 by 38 mm in outside diameter. Within the cell and under a dry, oxygen-free argon atmosphere, a LiCl-KCl eutectic mixture and the cathode depolarizer to be tested were compartmented by two small tubes with fritted glass bottoms which acted as salt bridges.

A spectrographically pure graphite rod in one tube, was used as the auxiliary electrode. The indicator electrode was a foil, a wire, or a rod of the electrode material under test. The indicator electrode, the reference electrode, and the thermocouple were placed in the other tube with fritted glass bottom containing the cathode material.

Substantial diffusion of the eutectic mixture into the cathode material compartment was the probable cause of the steady drifts of cathode potentials repeatedly observed using this experimental setup. The cell could not be used for the testing of volatile cathode materials.

In another experimental setup used in this study, the cell components were contained within a Pyrex H-shaped apparatus (Figure 7). The auxiliary electrode was compartmented from the rest of the cell using a Pyrex tube with a fritted glass bottom which was inserted in one arm of the cell. The other arm contained the indicator electrode, the reference electrode, and a thermocouple.

The auxiliary electrode compartment contained a small amount of LiCl-KCl eutectic. The main compartment received the cathode material to be tested. The diffusion of the eutectic mixture into the catholyte was slow. However, the setup was found unsuitable for testing volatile cathode depolarizers such as bismuth chloride.

In the experimental setup shown in Figure 8 the cathode material was contained in a Pyrex tube 260 by 12.7 mm in inside diameter. The indicator electrode was a gold wire 25 mils in diameter projecting 16.7 mm from the closed end of a Pyrex tube 270 by 3.2 mm in outside diameter. The total projected area of the gold electrode was 1/3 cm^2.

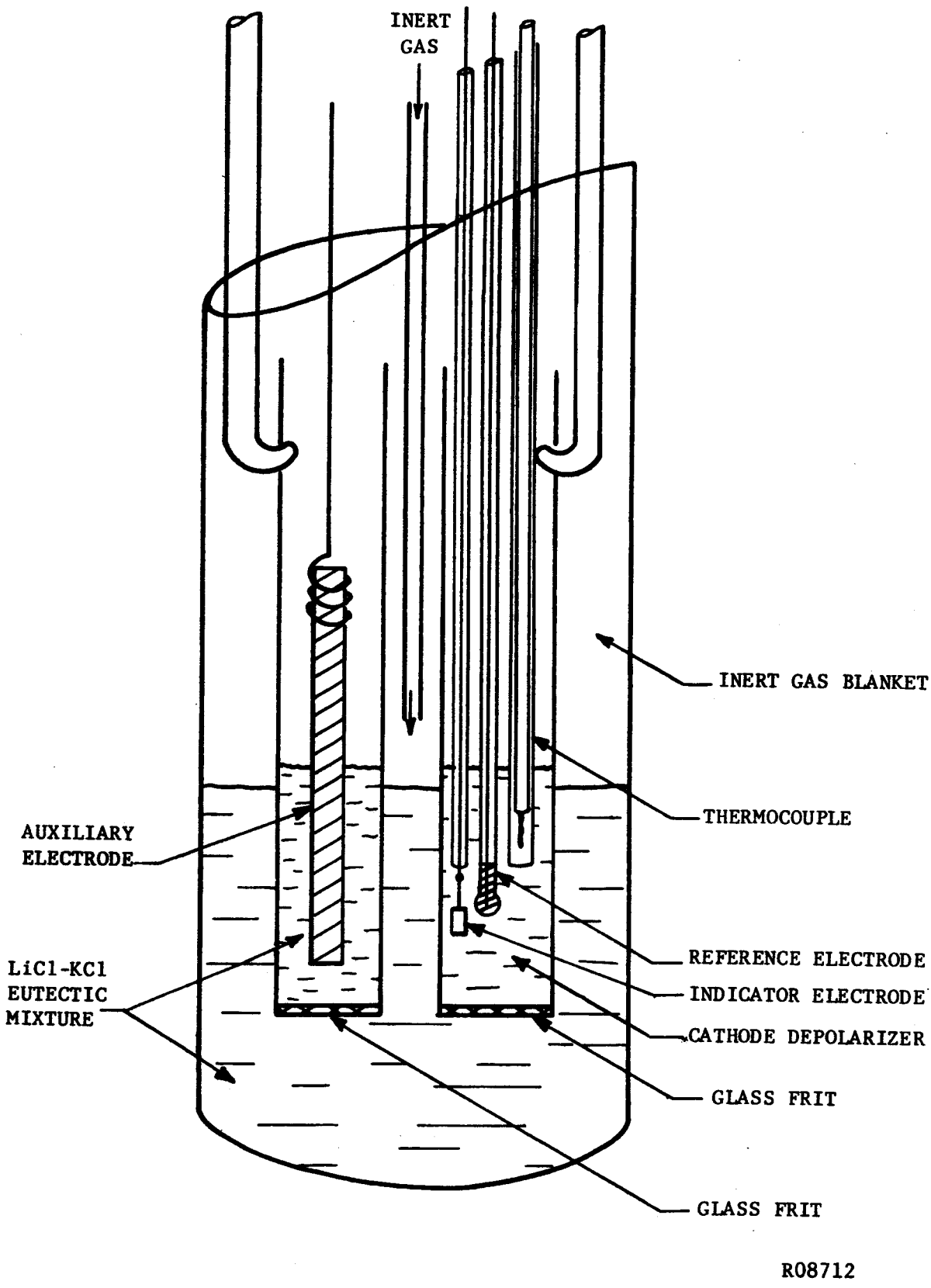

FIGURE 6. ELECTROLYSIS CELL

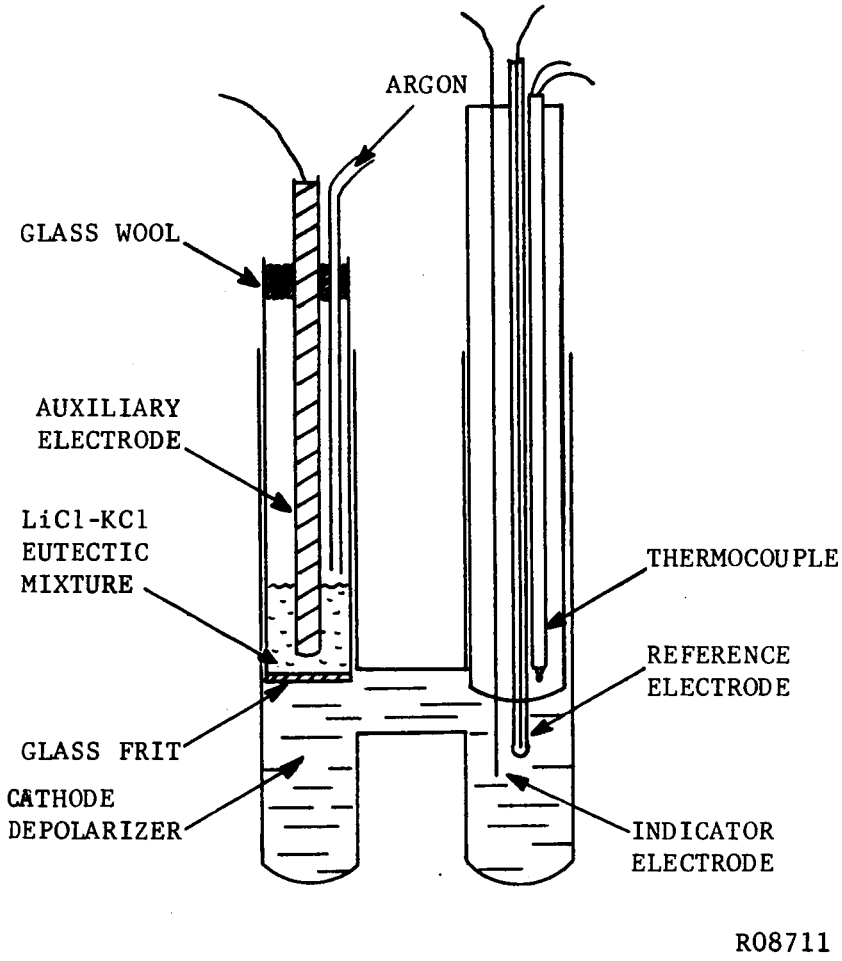

FIGURE 7. ELECTROLYSIS CELL

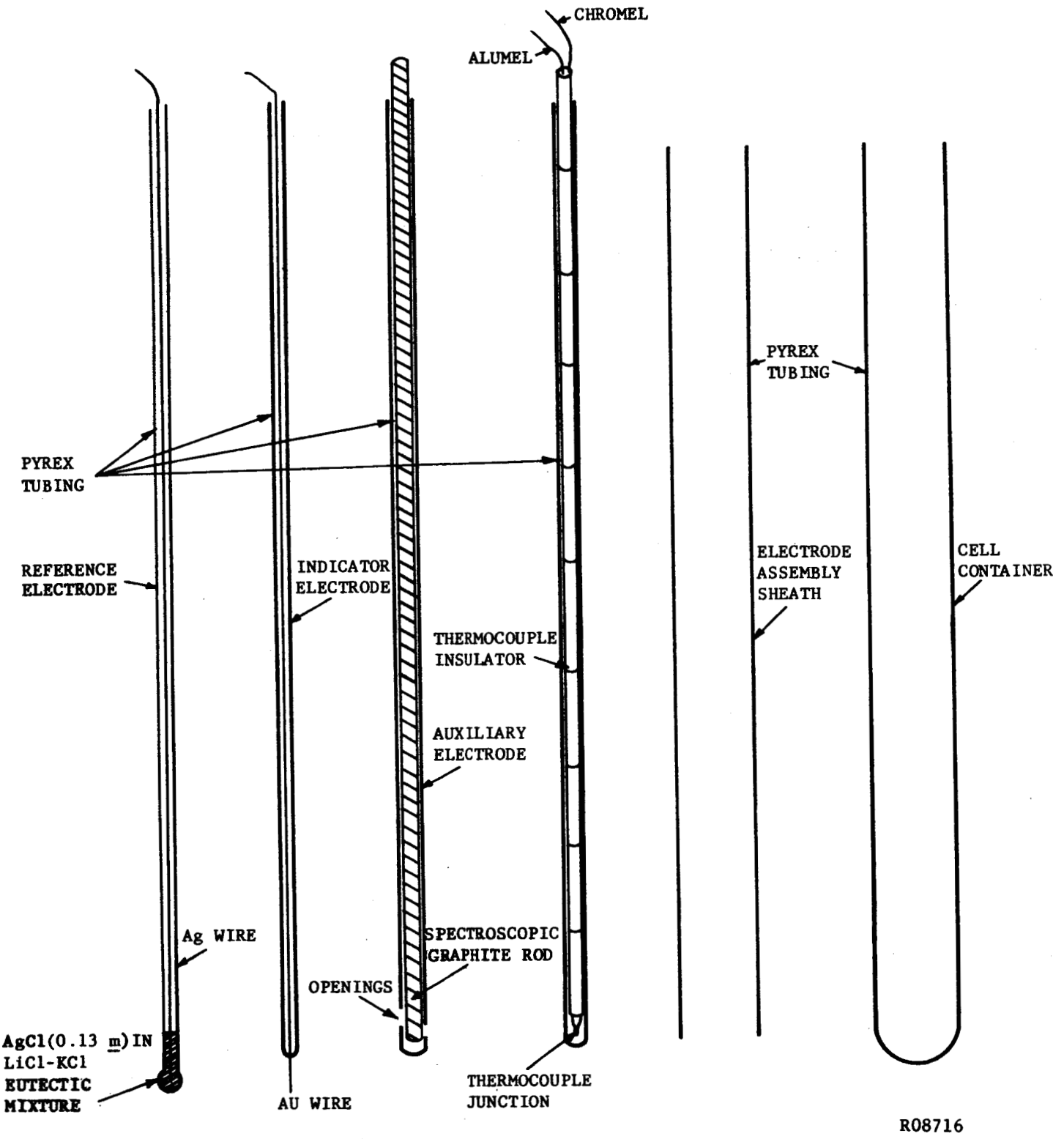

FIGURE 8. ELECTROLYSIS CELL AND COMPONENTS

The auxiliary electrode was a spectroscopic graphite rod 1/8-inch in diameter and 12 inches long. The density of the material was 1.9 g/cm^3. The rod was inserted in a Pyrex tubing 290 by 6 mm in outside diameter closed at the lower end and provided with side openings cut near the closed end with a diamond wheel. The reference electrode was identical in design with that described below.

The thermocouple was of the ISA type K (chromel-alumel junction). The wires, 12.5 mils in diameter, were inserted in short sections of two holes, round section refractory insulator 2.4 mm in diameter. The thermocouple sheath was made of Pyrex tubing 280 by 4.2 mm in outside diameter.

The electrodes and the thermocouple were fitted snugly in a Pyrex tubing 270 by 12.7 mm in outside diameter. The electrode assembly could be inserted with little friction in the cell container.

This cell was found satisfactory for experiments with volatile electrolytes.

f. Reference Electrode

The reference electrode system may be represented as follows:

$$\text{Ag} \;\Big/\; \begin{matrix}\text{AgCl (0.13}\underline{\text{m}}\text{)} \\ \text{KCl-LiCl (55-45 W/W)}\end{matrix} \;\Big/\!\!\Big/\; \text{glass}$$

The half cell was constructed from 3.2 mm outside diameter Pyrex tubing about 300 mm long, closed, and slightly blown at one end to reduce the wall thickness. The tube was heated to 130°C, vented with dry inert gas, then placed in a dry-box where a few milligrams of the premixed powder of AgCl and KCl-LiCl eutectic mixture was dropped to the bottom of the tube and the silver wire was inserted.

This electrode could not be used in the study of ferric chloride which melts and boils at temperatures below the melting point of the solvent in the Ag-AgCl reference electrode. However, the potential of the Au-$FeCl_3$ system at 290°C could be obtained indirectly with respect to Ag-AgCl electrode as follows:

The voltage of the system

$$\text{Au} \;\Big/\; \text{FeCl}_3 \;\Big/\!\!\Big/\; \text{glass} \;\Big/\!\!\Big/\; \text{BiCl}_3 \;\Big/\; \text{Au} \qquad (1)$$

was measured at 290°C.

The voltage of the system

$$\text{Au} \;\Big/\; \text{BiCl}_3 \;\Big/\!\!\Big/\; \text{glass} \;\Big/\!\!\Big/\; \begin{matrix}\text{AgCl(0.13}\underline{\text{m}}\text{)} \\ \text{KCl-LiCl (55-45 W/W)}\end{matrix} \;\Big/\; \text{Ag} \qquad (2)$$

was determined at a temperature range between 330° and 390°C.* A linear voltage-temperature relationship was observed in this range. Thus, assuming the linearity extending to 290°C, the voltage at the latter temperature was obtained by graphical extrapolation of the straight line. The potential of the Au-$FeCl_3$ half-cell with respect to Ag-AgCl reference electrode at 290°C can then be obtained by adding algebraically the voltages of the systems (1) and (2).

2.1.2 CHEMICALS

The following chemicals were obtained as the commercially available anhydrous materials. They were vacuum desiccated and kept in a dry box before use.

a. Cathode Depolarizers

Cupric chloride, from Baker & Adamson; purity 99.0 percent

Cuprous chloride, from J. T. Baker; purity 92.5 percent

Bismuth trichloride, from J. T. Baker; purity 99.7 percent

Silver chloride, from J. T. Baker; purity 99.0 percent

Ferric chloride, sublimed powder from Matheson, Coleman and Bell

Potassium chromate, from J. T. Baker; purity 99.6 percent

Potassium dichromate, from Mallinckrodt Chemical Works; purity 99.5 percent

b. Cathode "Diluents"

Calcium chloride, from J. T. Baker; purity 96.6 percent

Bismuth metal, from J. T. Baker; purity 100 percent

c. Solvent

The eutectic mixture of lithium chloride - potassium chloride was used as the solvent for potassium chromate. Chlorine was used to remove water from the LiCl-KCl eutectic (40).

*Although the lower limit of the temperature range investigated was below the melting point of the solvent in the reference electrode, the recording of the potential remained steady and no break in the linearity of the temperature-potential relationship was observed. It may be of interest to extend this investigation to even lower temperatures.

2.1.3 EXPERIMENTAL PROCEDURE

In all cases, potential measurements were made both on open circuit and on drain at current densities of 0.015 and 0.150 amperes per square centimeter. All potentials are reported with respect to a Ag - 1m AgCl electrode in LiCl-KCl eutectic. Spectrographic graphite was used as the auxiliary electrode. New electrodes were prepared for each experiment.

In the cell using a zeolite solid electrolyte as described in Reference (47), Ca^{++} will be transferred across the zeolite and into the cathode compartment as a result of the electrolytic conduction process. The cathodic reaction will also remove the cathode depolarizer. The net results of these two processes is a dilution of the catholyte with $CaCl_2$. Therefore, the properties of the cathode depolarizers were determined both as pure salts and "diluted" with $CaCl_2$. The results are summarized as follows.

a. Bismuth (III)

The experimental results for bismuth chloride as the pure molten salt and mixed with calcium chloride are summarized in Figure 9. The potential scale given in this figure is with respect to a Ag-0.13m AgCl electrode (Paragraph 2.1.1.a) which was used as a working reference electrode. To convert these potentials to the Ag-1m AgCl scale, 0.127 volt must be subtracted from those given in the figure.

Pure molten $BiCl_3$ at 380°C gave an initial open circuit potential of +0.84 volt (vs Ag-1m AgCl) on a gold electrode. After the initial current passage, the open circuit potential was found to be +0.78 volt. Significant changes in the initial open circuit potentials were observed with many of the systems studied. This change can be easily explained by recognizing that before the initial current drain there was no reduced form of the cathode depolarizer present in the system. Consequently, the potential determining couple was very poorly defined and the system was not well poised. Upon current drain, the reduced form of the cathode depolarizer was present and the potential of the system became better stabilized. In the pure molten $BiCl_3$ system, the average polarizations were about 45 and 110 millivolts at current densities of 0.015 and 0.150 amps/sq cm, respectively. The manner in which the potential changed when the current drain changed and the experimental setup suggested that a considerable portion of the observed polarization was due to iR drop in the electrolyte between the indicator and reference electrodes.

Figure 9 also shows the effect of various concentrations of calcium chloride "diluent" upon the performance of the $BiCl_3$ system. Compositions are given in mole percent. In addition to larger iR drops, considerable polarization was apparent particularly at 0.150 amps/sq cm. These observations can be partially explained by the insolubility of $CaCl_2$ in molten $BiCl_3$ at these temperatures. Although a complete phase diagram for the $BiCl_3$-$CaCl_2$ system is not available, the phase diagram for AgCl-$CaCl_2$ and CuCl-$CaCl_2$ (Figure 10) would suggest that only about 15 to 20 mole percent of $CaCl_2$ would be soluble.

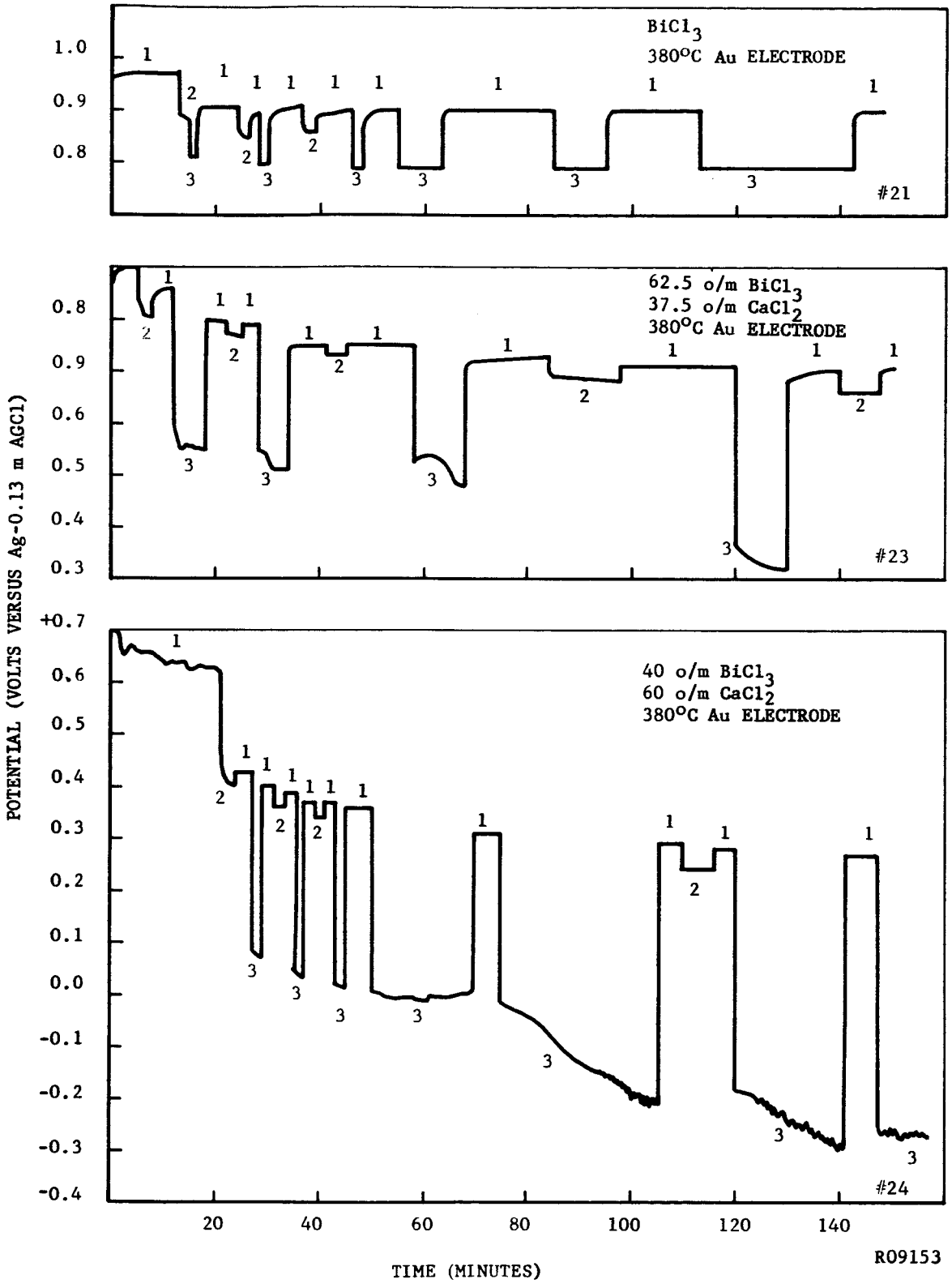

FIGURE 9. $BiCl_3$ REDUCTION. EFFECT OF DILUENTS

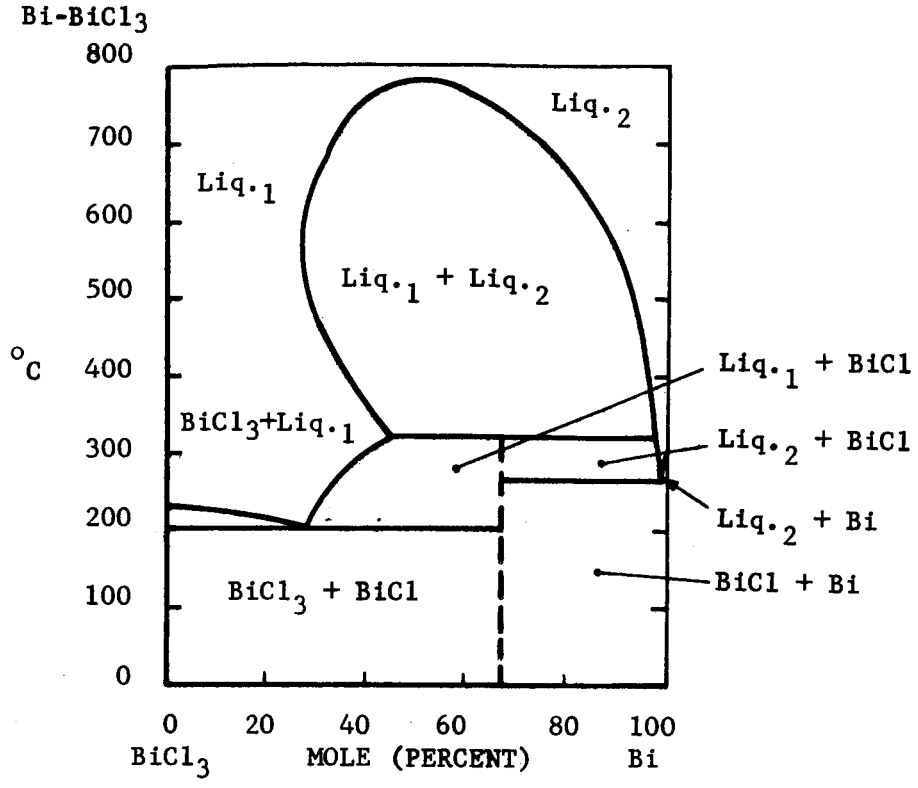

S. J. Yosim, A. J. Darnell, W. G. Gehman and S. W. Mayer, J. Phys. Chem., 63, 231 (1959).

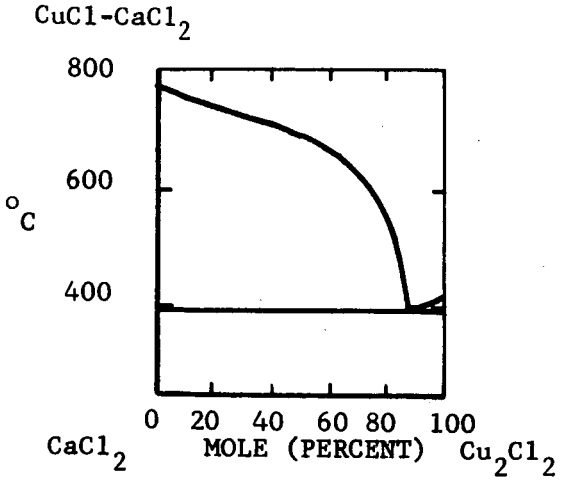

Otto Menge, Z. anorg. Chem., 72, 209 (1911).

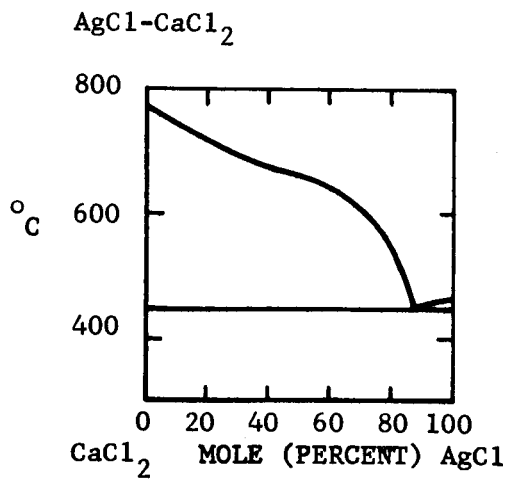

Otto Menge, Z. anorg. Chem., 72, 204 (1911).

R09155

FIGURE 10. PHASE DIAGRAM FROM REFERENCE 50

The phase diagram for the Bi-$BiCl_3$ system (Figure 10) shows that the reduction product of $BiCl_3$ at these temperatures will form a single liquid phase with $BiCl_3$ until approximately one-third of the $BiCl_3$ is reduced. This single liquid phase is probably a solution of BiCl in $BiCl_3$. The BiCl is either formed directly by the two electron reduction of $BiCl_3$:

$$BiCl_3 + 2e \longrightarrow BiCl + 2Cl^-$$

or by a three electron reduction of $BiCl_3$

$$BiCl_3 + 3e \longrightarrow Bi + 3Cl^-$$

followed by reaction of the Bi with excess $BiCl_3$

$$2Bi + BiCl_3 \longrightarrow 3BiCl$$

Regardless of the manner in which the reaction occurs, the formation of a soluble reduction product would be expected to affect the potential of the system (Nernst equation). Figure 11 shows the effect of both $CaCl_2$ and Bi metal upon the $BiCl_3$ system. The compositions were chosen on the basis of the following assumptions:

(1) An initial three-fold excess of $BiCl_3$

(2) A three electron reduction for $BiCl_3$

(3) Metallic Bi and $CaCl_2$ appear in equivalent amounts.

The Bi-$BiCl_3$ phase diagram and electrochemical studies of this system (48) suggests that the assumption regarding the number of electrons in the reduction is incorrect.

Examination of the gold electrodes after tests showed extensive degradation of the gold. Gold and metallic Bi are known to form liquid alloys at these temperatures (49). It is possible that the stability of the liquid Au-Bi alloy would promote the reaction

$$BiCl + Au \longrightarrow Bi + AuCl$$

and produce the metallic Bi necessary for alloy formation. Thus, it appears that the poorer performance of these systems is due to a degradation of the gold electrode by alloy formation with a corresponding increase in current density.

No degradation was noted with a tungsten electrode even at 425°C. (Figure 11). Polarization was slight and appeared to be essentially of a resistive nature. The shift of the electrode potential in the negative direction when Bi is added to the system is quite apparent. No explanation is given at the present time for the shift of the electrode potential in the first twenty minutes of testing.

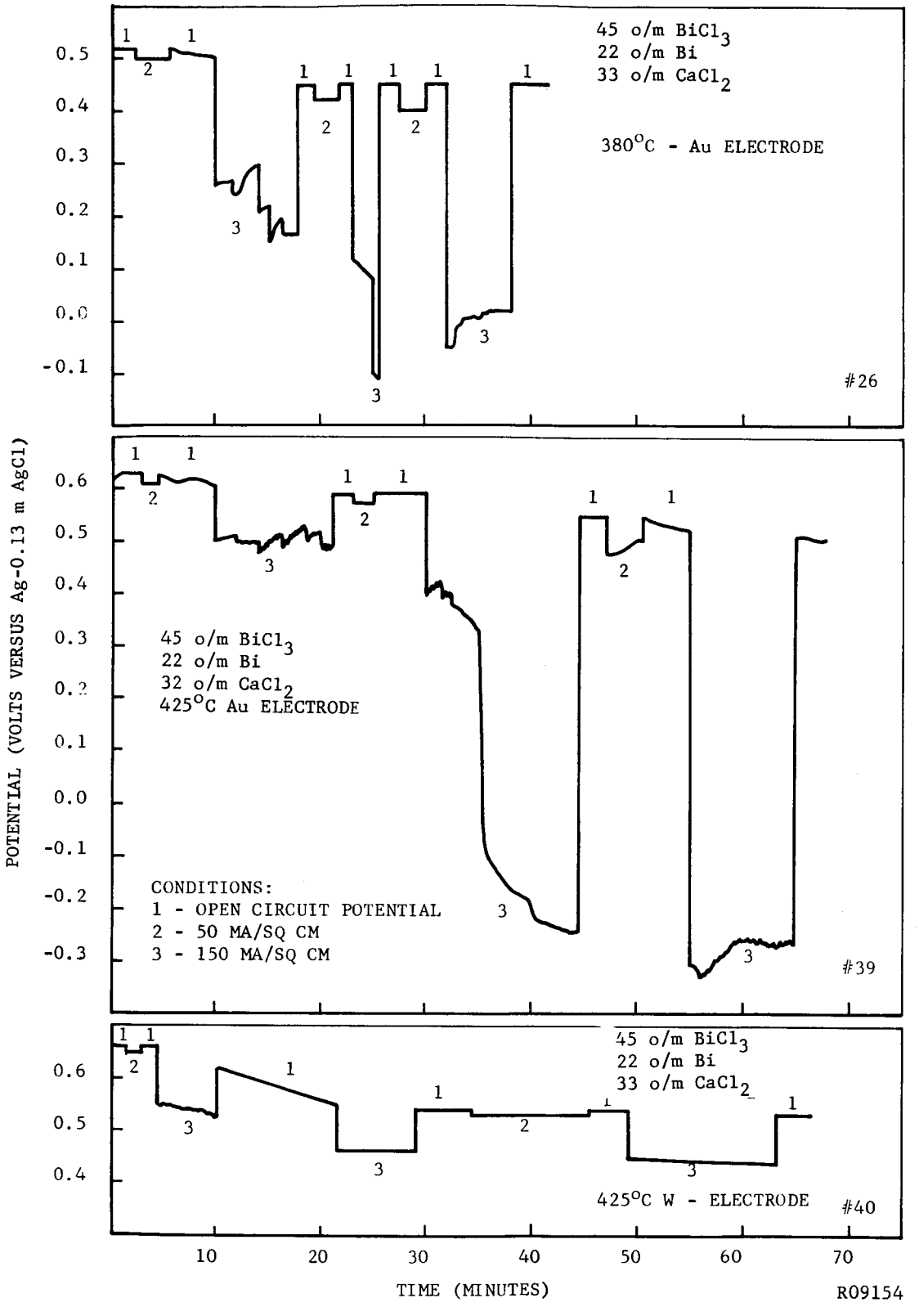

FIGURE 11. $BiCl_3$ REDUCTION. EFFECT OF DILUENT, TEMPERATURE, AND ELECTRODE

With all cells containing $CaCl_2$, some solid material was present at the operating temperature. This solid material was probably undissolved $CaCl_2$. With the ternary system ($BiCl_3$-Bi-$CaCl_2$), solid material was observed at temperatures as high as 640°C. Upon cooling of these mixtures, more solid material was formed and at 182°C an inflection appeared in the cooling curve and the mixture became completely solid.

b. Iron (III)

Pure ferric chloride quickly deteriorated both the gold indicator electrode and the graphite auxiliary electrode although the metal chloride did not appear to have melted at the operating temperature of the cell (290°C). The Au-$BiCl_3$ half cell was used as the reference electrode and the potential obtained was converted with respect to Ag-AgCl 0.13 m or 1.0 m in LiCl-KCl as described previously. An open circuit potential of +1.13 volts was thus obtained. No current could be passed through the cell because of the very high cell resistance.

c. Copper (I)

The open circuit potential of molten cuprous chloride at 450°C on gold and copper electrodes was +1.11 and +0.51 volts, respectively. With both electrodes these potentials shifted to +0.16 volt (vs 0.13m AgCl) after a short period of current flow. Little polarization other than iR drop was noted at 0.015 and 0.150 amps/sq cm. Figure 12 shows results obtained with a gold electrode in molten CuCl at 445°C. The slight decrease in potential with time was probably due to dilution of the CuCl by molten KCl-LiCl. The electrolysis cell shown in Figure 6 was used to obtain these curves.

The high initial potential is attributed to the presence of Cu(II) present as an impurity in the cuprous chloride. Polarographic analysis showed that the CuCl contained approximately 7 percent Cu(II). The effect of the Cu(II) can be removed by cathodic reduction.

d. Copper (II)

No lengthy experiments could be carried out with molten cupric chloride since all the electrode materials tested so far deteriorated within a few minutes in the melt. Using the cell shown in Figure 6, open circuit potentials of +0.88 volt and +1.32 volts were measured on gold and graphite, respectively. It appeared that some dilution of the molten $CuCl_2$ with LiCl-KCl eutectic mixture occurred during these experiments. Using a latter cell design (Figure 8), open circuit potentials of +1.40 volts and +1.45 volts were measured on gold and graphite, respectively, at 525°C. Initially, very little polarization was observed at 0.015 and 0.150 amp/cm^2. No extensive polarization experiments could be conducted because of the deterioration of the electrodes.

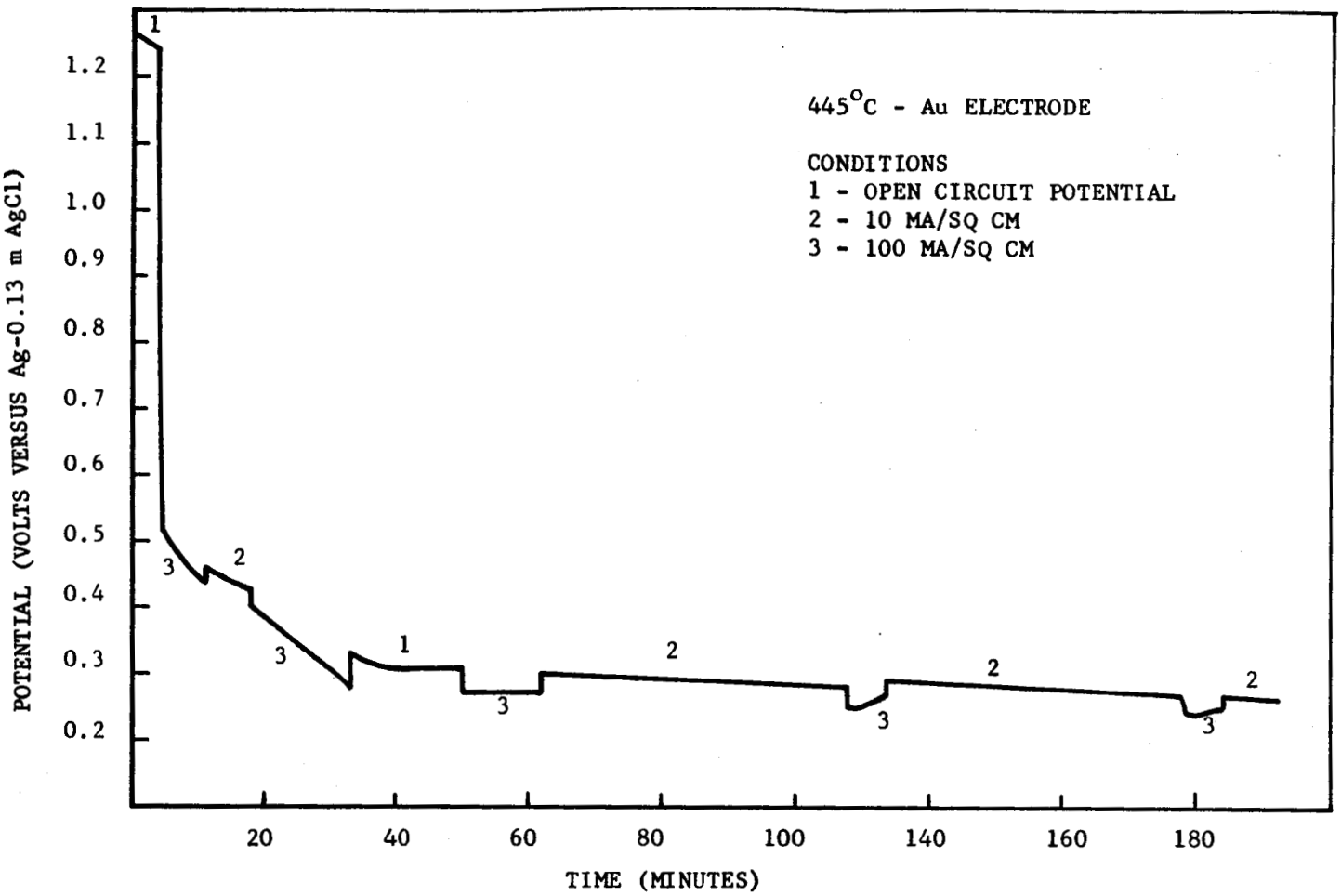

FIGURE 12. CuCl REDUCTION

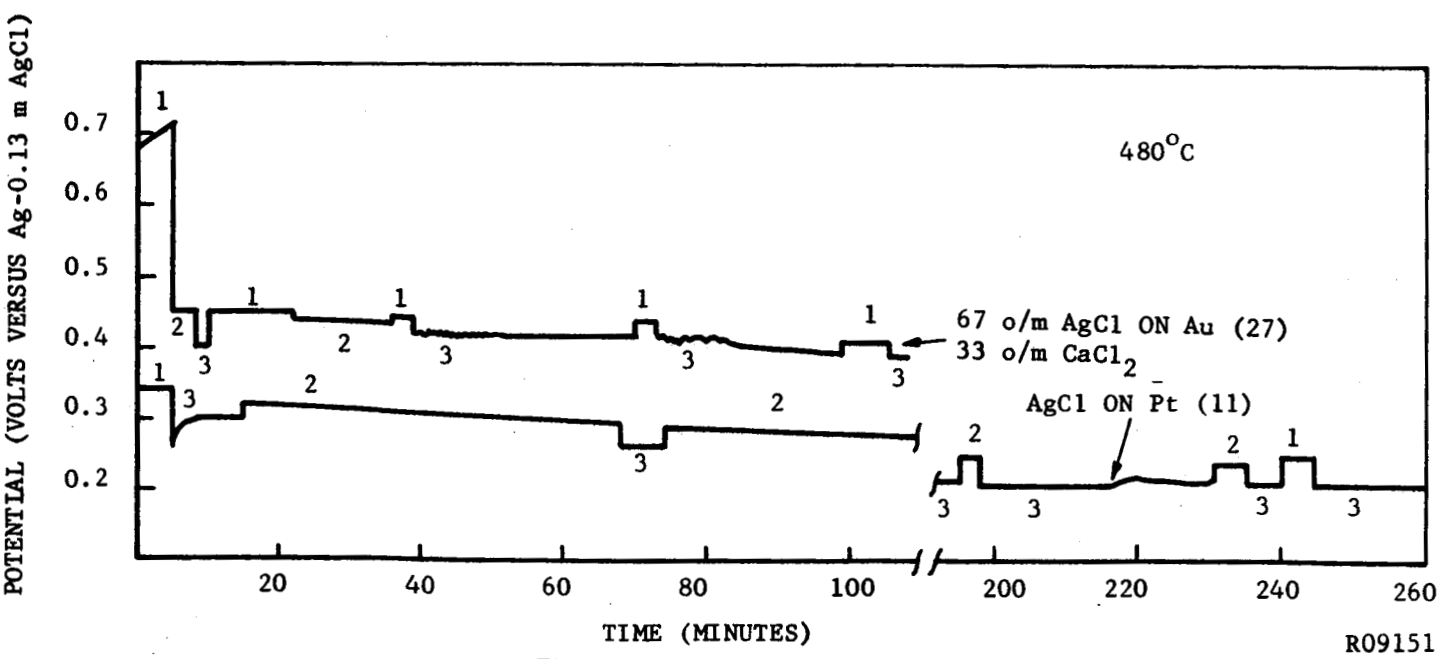

FIGURE 13. AgCl REDUCTION

e. Silver (I)

Pure molten silver chloride gave an open circuit potential of +0.21 volt on a Pt electrode at 480°C. Little polarization was observed at current densities of 0.015 and 0.150 amps/sq cm. The slow decrease in potential was probably due to dilution with LiCl-KCl. A mixture of 67 mole percent AgCl and 33 mole percent $CaCl_2$ (1 to 1 equivalent ratio) gave a steady state open circuit potential of +0.32 volt on a Au electrode. No reason can be given at this time for the higher potentials in the AgCl-$CaCl_2$ systems. Experimental curves for these systems are given in Figure 13. As would be expected from the phase diagram for the AgCl-$CaCl_2$ system (Figure 10), the mixture of AgCl and $CaCl_2$ contained a solution of $CaCl_2$ in AgCl and some undissolved $CaCl_2$.

f. Chromium (VI)

Pure molten potassium dichromate and a 6.65 mole percent solution of potassium chromate in LiCl-KCl eutectic mixture gave open circuit potentials of +0.76 volt and +0.42 volt, respectively, on gold at 450°C. Under current drain, the polarization increased rapidly to negative potential values. Potential-time curves for these systems at low current densities are shown in Figures 14 and 15. The extensive polarization is quite apparent. A dark green deposit was found on the electrodes in both experiments. A portion of the polarization appears to be due to very high resistance of this film.

2.1.4 SUMMARY AND DISCUSSION

All pure molten metal chlorides tested heretofore showed very little polarization, if any, under the present test conditions.

Mixing some of these chlorides with equivalent amounts of by-products assumed to contaminate the cathode material during normal cell discharge caused substantial open circuit potential shifts toward negative values, and rapidly increasing polarization under current drains. Since these mixtures were more or less in the solid phase at the operating temperature of the cell, concentration polarization would be expected.

The dark greenish deposit observed on gold in molten potassium dichromate and in a solution of potassium chromate in fused LiCl-KCl eutectic mixture is likely an oxide of chromium. The film formed under current drain, and produced a large iR drop.

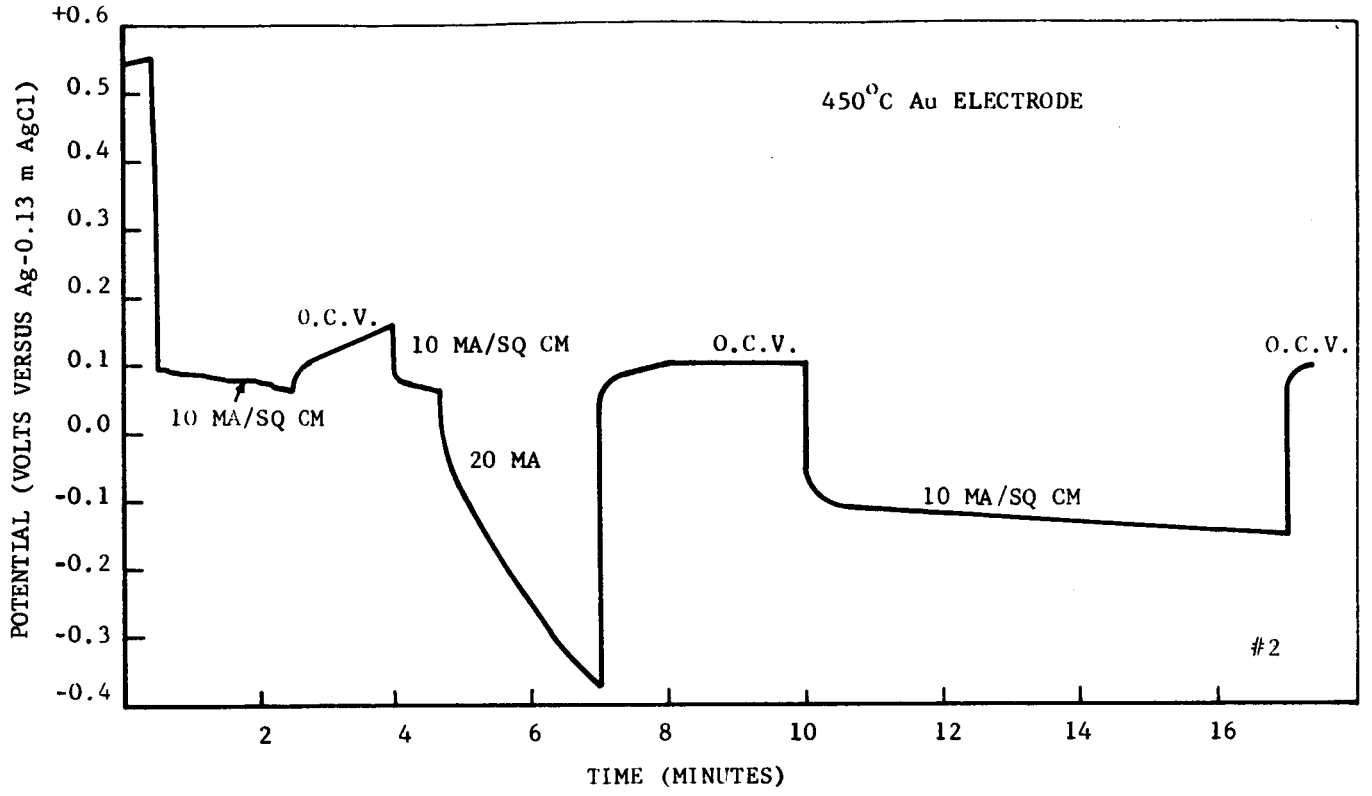

FIGURE 14. REDUCTION OF 6.65 MOLE PERCENT $K_2Cr_2O_7$

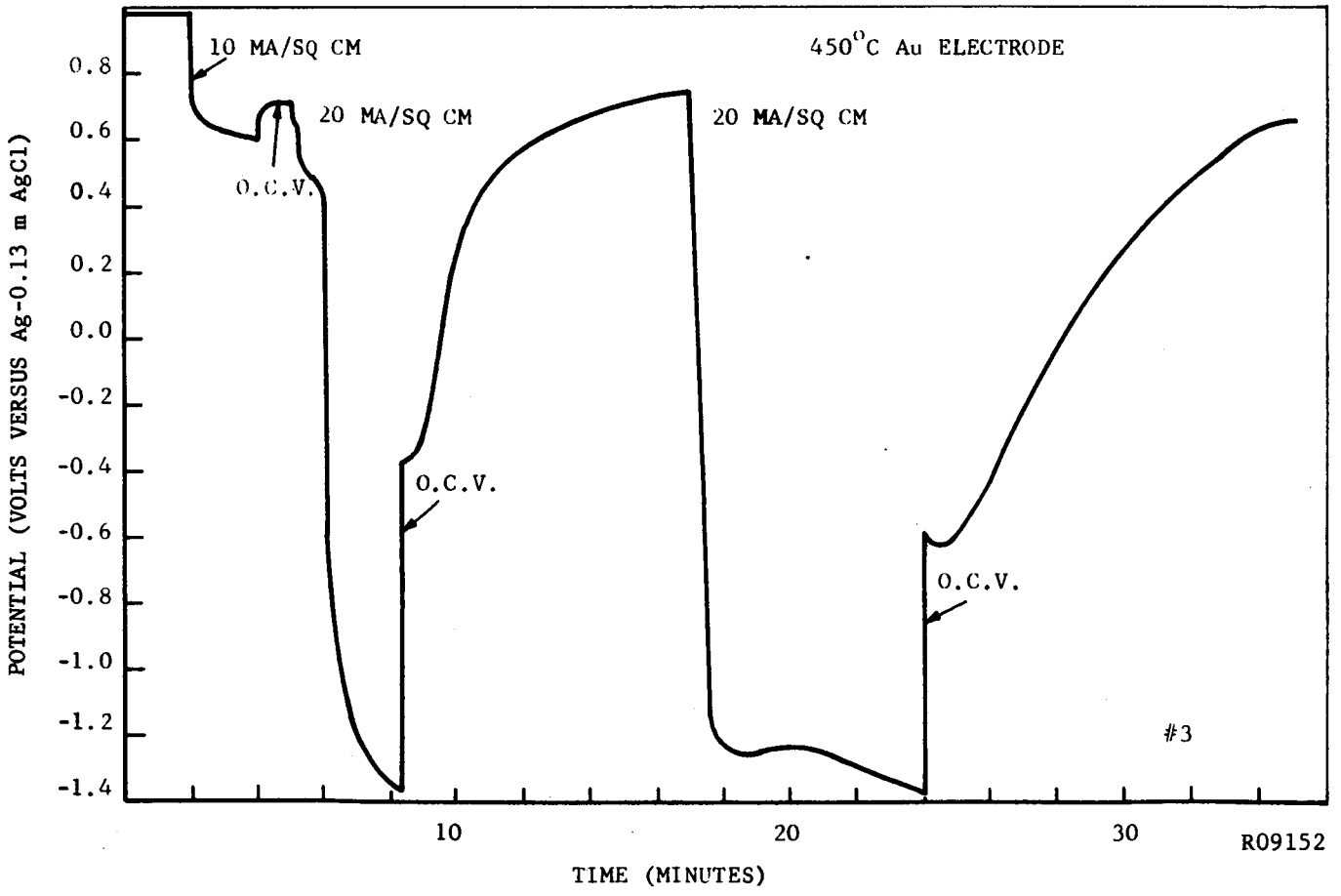

FIGURE 15. REDUCTION OF MOLTEN $K_2Cr_2O_7$

2.2 ZEOLITES

The experimental work on zeolites can be divided into three areas:

(1) Cathode weights for solid state batteries

(2) Fabrication and conductivity of zeolite membranes

(3) Ion exchange studies

2.2.1 SOLID STATE BATTERY

One of the principal problems associated with most battery systems for aerospace applications is to find suitable method to hermetically seal the battery and prevent leakage and loss of electrolyte. This problem becomes particularly severe as the operating temperature of the battery increases. The use of ion exchange membranes, both organic and inorganic, as solid electrolytes in fuel cells represents an attempt to solve this problem by minimizing the amount of liquid present.

The synthetic zeolites, because of their ionic conductivity, particularly at high temperatures, are suitable for use as solid electrolytes. In addition, zeolites which have been exchanged with reducible metal ions such as Ag^{+}, Cu^{++}, Hg^{++}, Ni^{++}, and Au^{+} can be used in a dual role as solid electrolyte and cathode depolarizer.

The electrical properties of zeolites discussed above, together with the fact that zeolite crystals can be very easily ion-exchanged with reducible metal ions, have made possible the preparation of a primary cell.[39] The features of such a cell are long life and operation over a wide temperature range. Since the only mass transfer across the lattice is the diffusing ions, it can be considered to be a true solid-state cell. To illustrate the principle, consider a cell made up from a catholyte $Ag^{+}Z^{-}$ bonded to $Na^{+}Z^{-}$ electrolyte which in turn is bonded to a Zn anode. Gold foil can be used as a current collector at the cathode. This cell can be represented as

$$Zn/Na^{+}Z^{-}/Ag^{+}Z^{-}/Au$$

This system can be compacted to small discs; for example, 1/2-inch diameter with 1/4-inch thickness. The zeolite segments in the system can be illustrated as follows:

The operation of the completely solid cell formed in this way can best be illustrated by the series of reactions at the various parts of the cell

Anode reaction $Zn \rightarrow Zn^{++} + 2e^-$

Cathode reaction $2\,Ag^+ + 2e^- \rightarrow 2\,Ag$

Electrolytic reaction $Zn^{++} + 2\,Ag^{++}Z^- \rightarrow Zn^{++}Z_2^- + 2\,Ag^+$

Other combinations of catholyte/electrolyte/anode systems are possible; for example,

$Zn/Ca^{++}\ Z_2^-/Hg^{++}Z_2^-/Au$

The power output of the system depends on the following factors:

(1) Temperature

(2) Type of phase and amount of absorption

(3) Type of catholyte

(4) Type of electrolyte and anode

Preliminary experimental results have been obtained with such a cell and indicate that it can operate from -79°C up to 700°C-800°C. Voltages in the range of 2 to 3 volts have been measured. These cells can be stacked together to form high-voltage solid-state batteries. An advantage of this type of porous crystal over the ion-exchange resins is their high electrochemical equivalent (700-750 coulombs/cc) and their tolerance to considerably higher temperatures, i.e., stability of some zeolites extends up to 1000°C.

The weight requirements of the cathode portion of such a solid state battery can be calculated. For 14 ampere-hours of operation, a total of 0.523 equivalents of the cathode would be required. A comparison of this amount of various cathode depolarizers is shown in Table IX. The amounts of cathode depolarizer required for 14 ampere-hours of operation were calculated with the assumption that the cathode depolarizer was reduced at 100 percent efficiency with the number of electron per molecule as given by the "n" value. No provisions have been made in the calculations for the amount of electrolyte which might be required with the conventional depolarizers. It appears that the active weight of a cathode composed of a zeolite containing a reducible cation will be heavier than that of a conventional depolarizer. However, it must be emphasized that the zeolite also serves as the electrolyte. When the electrolyte requirements of conventional depolarizers are taken into account, the use of a zeolitic cathode becomes more attractive. In addition, it would appear that the zeolite type of cell might be easier to fabricate and might contain less inert materials.

TABLE IX

COMPARISON OF CATHODE DEPOLARIZERS

Cathode Depolarizer	n	Equivalent Weight, grams	Weight for 14 ampere-hours
Type A Zeolite in Ag^{+} form	1	226.9	119
Type A Zeolite in Cu^{++} form	2	149.8	79
Type A Zeolite in Ni^{++} form	2	147.42	77
Type X Zeolite in Ag^{+} form	1	237.9	124
Type X Zeolite in Cu^{++} form	2	161.8	85
$CuCl_2$	2	67.2	35
$FeCl_3$	1	162.2	84
$BiCl_3$	3	105.1	55
AgCl	1	144.3	75
CuO	2	39.8	20.8

2.2.2 FABRICATION AND CONDUCTIVITY OF ZEOLITE MEMBRANES

Initial efforts will be directed towards preparation of zeolite membranes by vacuum hot pressing[16]. A chamber has been constructed in which the zeolite powders will be compacted between two gold foil electrodes. The foil electrodes will be used for the conductivity measurements. A sketch of the chamber is given in Figure 16. The chamber can be evacuated to a pressure of a few microns while heating the sample. The vacuum heating will dehydrate the zeolite powders before compacting. Dehydration is very important since the zeolites can lose their crystallinity if they are pressed while fully hydrated. The typical compacting procedure will be to place the powdered zeolite and the foil electrodes in the carbolloy die in the chamber. The chamber will be evacuated and heated to 150 to 200°C for approximately one hour. A pressure of 30,000 to 50,000 psi is then used to form coherent, dense, and structurally intact compacts. Densities close to 90 percent of the single crystal value have been obtained by this method.[16]

The compacts with attached gold foil electrodes will then be transferred to the conductivity cell. The conductivity of the zeolites will be determined as a function of zeolite type, cation form, temperature, and nature of gas phase in contact with the zeolite. From the Arrhenius plots (see Figure 2) of conductivity versus temperature, the activation energy for the conduction process for the particular cation in the crystal lattice will be determined.

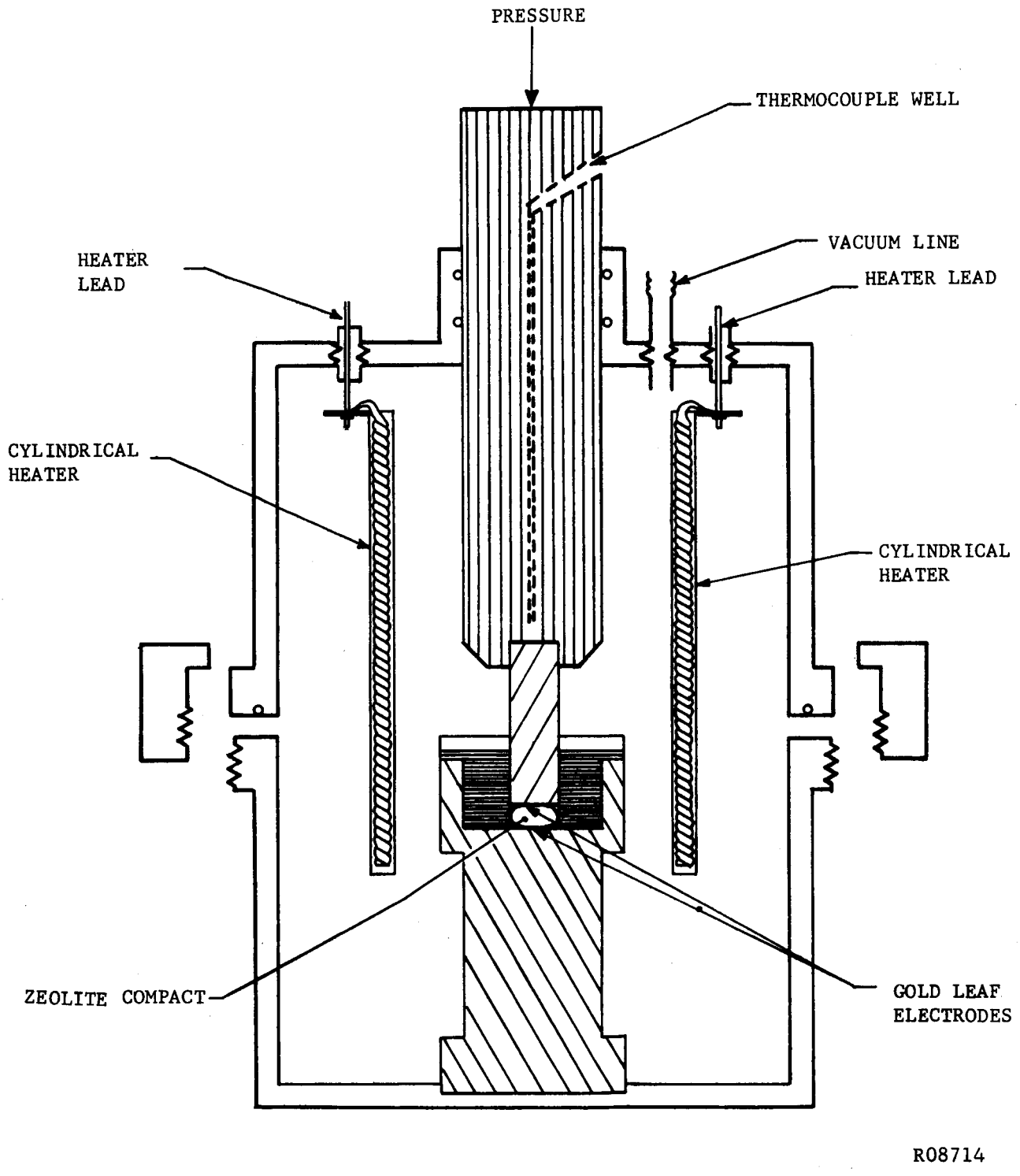

FIGURE 16. HEATED VACUUM CHAMBER FOR COMPACTING ZEOLITES

An overall view of the conductivity cell is given in Figure 17. A more detailed drawing of the lower electrode and heater is given in Figure 18. The interior of the cell (heater and electrode supports) are made of quartz to permit measurements at temperatures up to 1000°C. The conductivity cell can also be used to determine the characteristics of the completely solid batteries.

A sample of Type X zeolite in the sodium ion form was compacted and subjected to conductivity measurements. The powder zeolite was placed between two gold leaf electrodes in vacuum chamber. The powder was allowed to dehydrate in the vacuum chamber for one hour at 150°C and approximately 10 microns pressure. After dehydration, the powder was pressed at 40,000 psi for 15 minutes. This produced easily handled pellets with tightly bonded gold electrodes.

The compacted zeolite pellets were transferred to the conductivity cell which was connected to the high vacuum system. Complete dehydration was achieved in the conductivity cell by slowly heating the pellet to 400°C while holding the pressure at about 10^{-6} mm of Hg. The pellet was subjected to these conditions for at least 16 hours.

The resistance of the pellet was determined as a function of temperature using an impedance bridge at 1000 cps. The specific resistivity was calculated from the measured resistance and the dimensions of the pellet. The results are shown in Figure 19. From the linearity of the plot, the compact appeared to exhibit ohmic behavior at the temperatures studied. This Arrhenious plot gave an activation energy of about 12 kilocalories per mole which is in good agreement with previously published data (16).

2.2.3 ZEOLITE EXCHANGE STUDIES

As a preliminary step to the determination of zeolite conductivity and to the preparation of solid state batteries for testing, attempts were made to exchange Type A zeolite with reducible metals ions.

A weighed portion of anhydrous Type A zeolite in the Na^+ form (NaA) was equilibrated with distilled water and air dried. The weight of the zeolite was found to increase 20.8 percent due to absorbed water. Exactly 0.1 equivalent of the hydrated zeolite was treated with 100 ml of a 1.0 N solution of $AgNO_3$ slightly acidified with HNO_3. At 15 minute intervals, the Ag^+ in solution was analyzed polarographically. No further decrease in the Ag^+ concentration was noted after the first 15 minute period. For the exchange reaction

$$NaA + Ag^+ \rightleftarrows AgA + Na^+$$

the apparent exchange constant, K'_{ex}, defined as

$$K'_{ex} = \frac{[Ag^+A][Na^+]}{[Na^+A][Ag^+]}$$

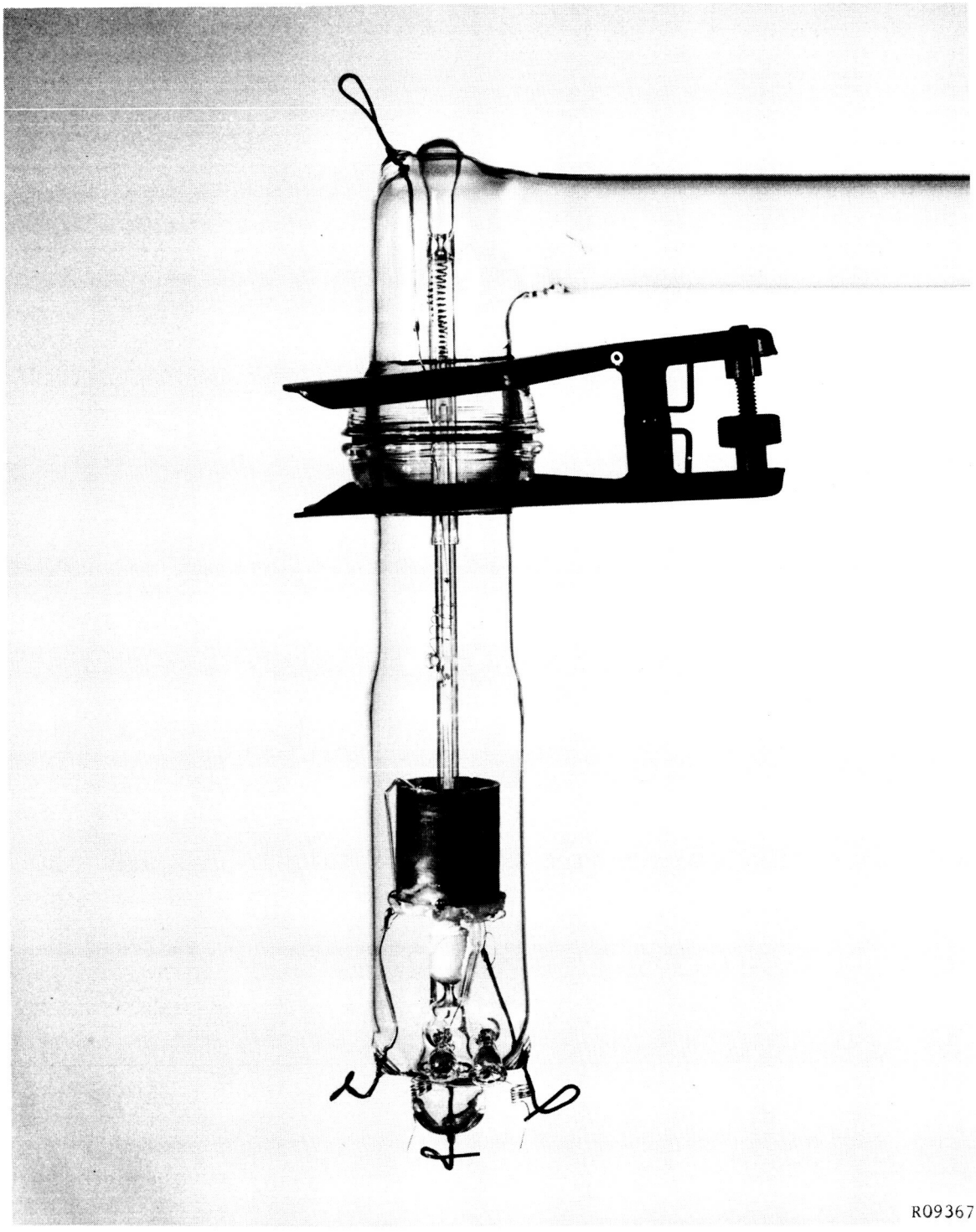

FIGURE 17. CONDUCTIVITY CELL

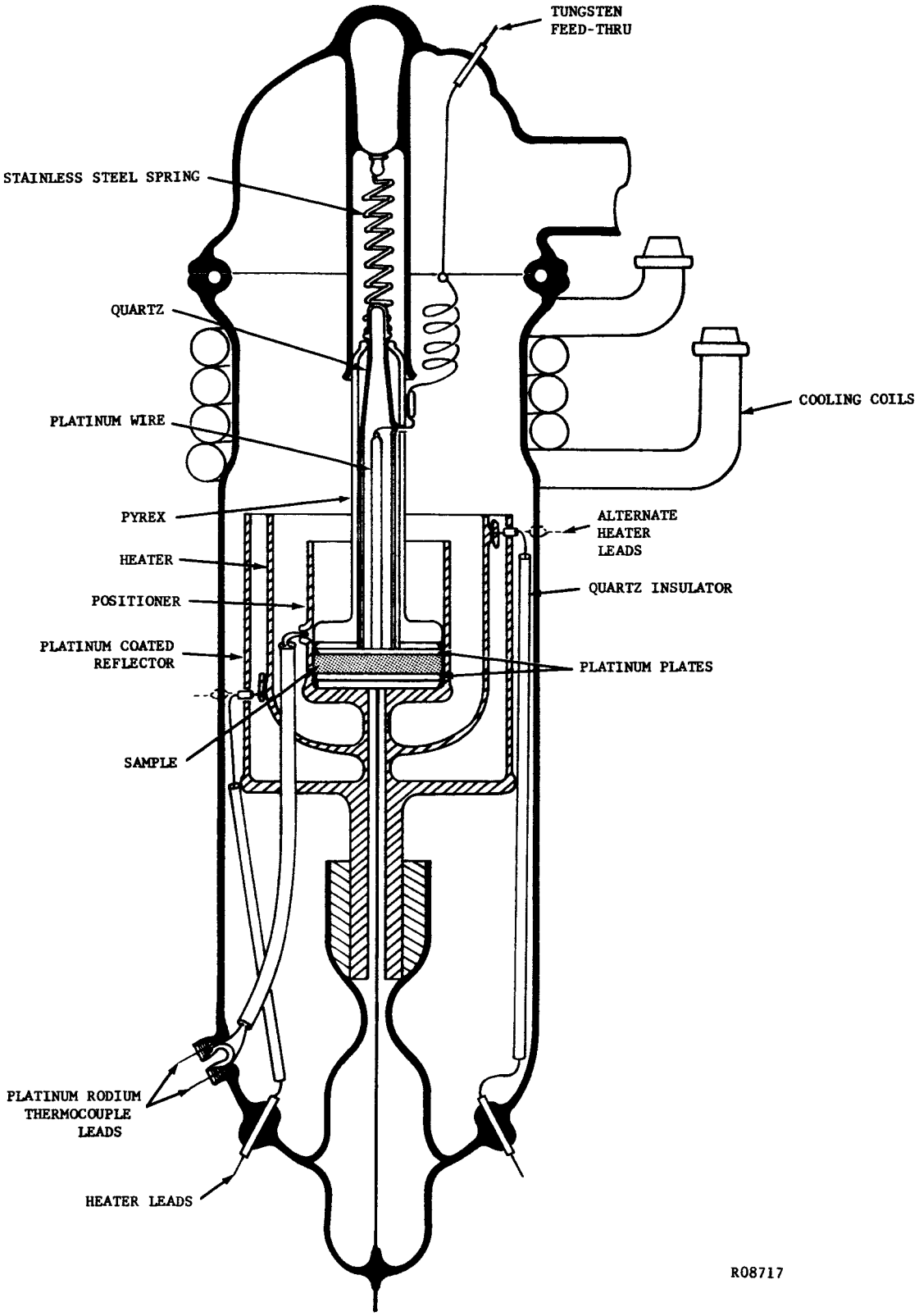

FIGURE 18. CONDUCTIVITY CELL DETAIL

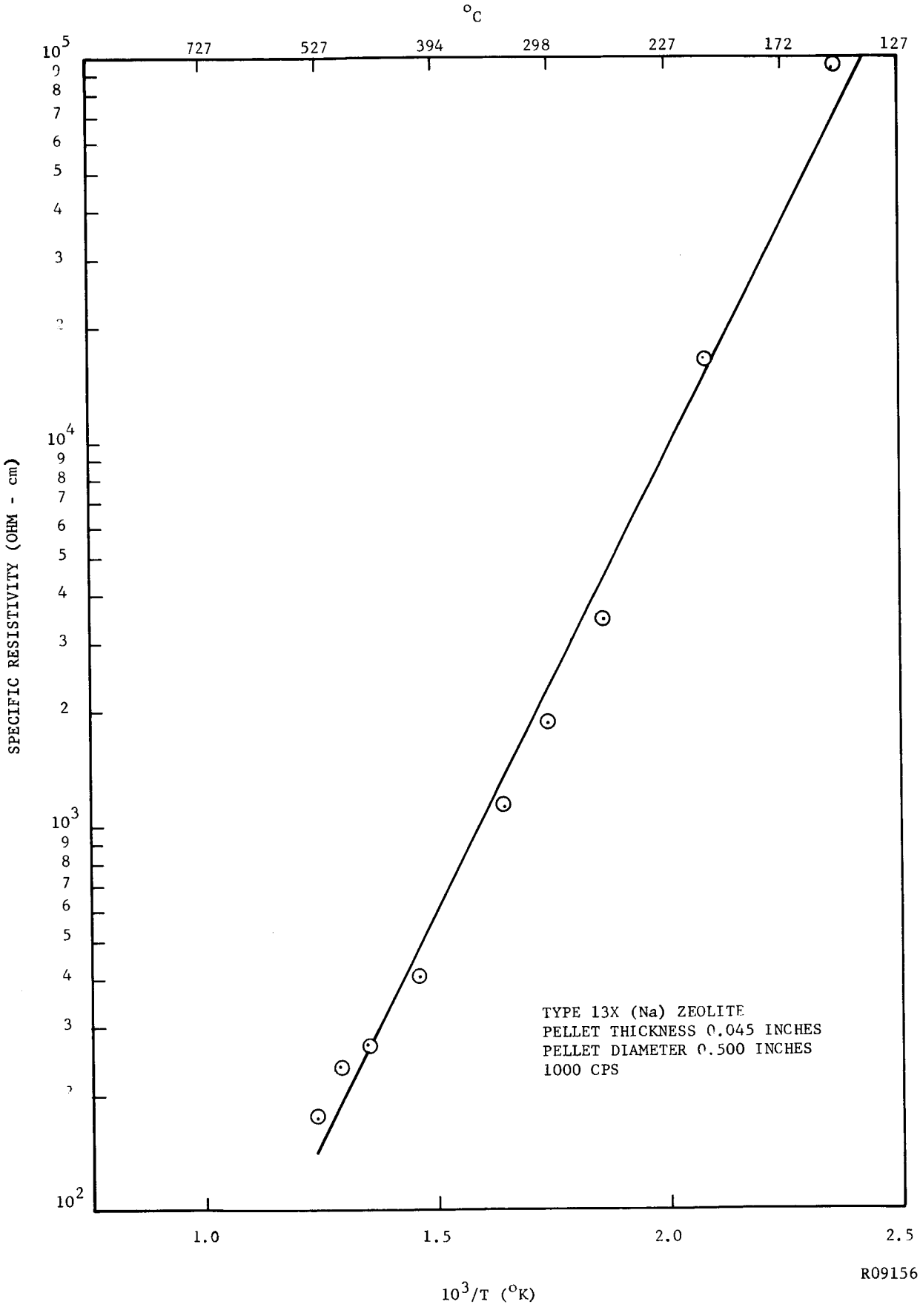

FIGURE 19. ARRHENIOUS PLOT

was 88.7 for the single exchange. This corresponded to a 90.4 percent exchange. A second treatment with $AgNO_3$ showed that the zeolite was 101 percent exchanged. After filtering and washing with distilled water until no trace of Ag^+ was detected in the filtrate, the zeolite was air dried. This white powder was then activated at 350°C under vacuum. The activated zeolite, now AgA, was bright orange.

A similar procedure was used in an attempt to form CuA_2. In this case the apparent exchange was much slower. The zeolite appeared to become more finely divided to such an extent that it was necessary to wash and separate the product in a centrifuge. The air dried powder was a very light blue in color. Upon vacuum activation at 350°C, the sample turned black. A reddish brown gas was noted when the cold trap cooled with liquid nitrogen was allowed to warm to room temperature. These observations seemed to indicate that exchange did not occur and that the reaction upon activation was simply the thermal decomposition of $Cu(NO_3)_2$ to CuO.

Power X-ray diffraction patterns were taken on a Norelco Philipp Spectrometer using Cu K_α radiation. Diffraction patterns of the original Type A zeolite, CuO, the silver exchanged zeolite and the copper treated zeolite were taken. The results are presented in Tables X and XI. The diffraction pattern for NaA and CaA_2 as reported in the literature [13] are also presented for comparison. The X-ray diffraction patterns indicate that all three zeolites, NaA, AgA and CaA_2, are simple cubics with a unit cell length of approximately 12.3 Å. For certain planes, the d spacings were not reported in the literature. These spacings were calculated from the crystal dimensions and are shown in parenthesis. The diffraction data indicates that Type A zeolite can be exchanged with Ag^+.

The diffraction pattern for the copper treated zeolite showed only the pattern for CuO imposed on a relatively high background. No peaks characteristic of the Type A zeolite were observed. The X-ray information along with the finess of the powder that was obtained indicate that the zeolite structure was broken down by treatment with $Cu(NO_3)_2$. This observation is confirmed in the literature.[13]

TABLE X

X-RAY DIFFRACTION DATA - TYPE A ZEOLITES

(h,k,l)	d, Å			
	NaA[13]	CaA2[13]	Type A As Received	"AgA"
100	12.294	12.243		
110	8.706	8.664	8.61	8.56
111	7.109	7.075	7.10	--
200	(6.06)	6.121	--	6.06
210	5.508	5.478	5.46	5.43
211	5.031	5.002	5.00	--
220	4.357	(4.33)	4.33	4.31
221, 300	4.107	4.084	4.08	4.07
310	(3.90)	3.875	3.87	3.87
311	3.714	3.696	3.70	3.68
222	(3.56)	3.539	--	3.53
320	3.417	3.398	3.40	3.41
321	3.293	3.276	3.29	3.26
400	(3.08)	(3.06)	3.06	3.04
410, 322	2.987	2.972	2.98	2.95
411, 330	2.904	2.888	2.89	2.88
331	(2.83)	(2.81)	--	--
420	2.754	2.741	2.74	2.73
421	2.688	2.676	2.68	--
332	2.626	2.614	2.615	2.61
422	2.515	2.502	2.50	2.50
430, 500	2.464	2.451	2.45	2.45
431, 510	(2.42)	(2.40)	--	2.40
511, 333	2.371	2.359	2.36	2.35
520, 432	2.289	(2.28)	--	2.27
521	2.249	2.238	2.24	--
440	2.177	2.166	2.17	2.16

d spacings in parenthesis calculated from the dimensions of the unit cell.

TABLE XI

X-RAY DIFFRACTION DATA FOR CuO AND Cu "EXCHANGED" TYPE A ZEOLITE

d, Å	
CuO	"CuA_2"
2.74	2.73
2.52	2.52
2.32	2.31
1.955	--
1.861	1.875
1.779	--
1.708	1.70
1.579	1.574
1.502	1.505
1.416	--
1.407	1.404
1.375	1.371

SECTION 3

FUTURE WORK

The determination of the electrochemical characteristics and freezing points of mixtures of possible cathode depolarizers and calcium chloride will continue. The cathode depolarizer to be studied will be AgCl, $BiCl_3$, $FeCl_3$, $CuCl_2$, and CuCl both as pure salts and as solutions in LiCl-KCl eutectic.

Crystalline zeolites containing various cations will be prepared and characterized by X-ray diffraction. Vacuum hot pressing and phosphate bonding will be investigated as possible methods of fabricating thin zeolite membranes. The ionic conductivity and other electrochemical properties of the zeolites will be determined. Solid state batteries using zeolites containing reducible cations as the cathode depolarizer will be fabricated and tested.

REFERENCES

1. R.M. Barrer, J. Chem. Soc., 1948, 127.

2. R.M. Barrer, Proc. Intern. Symposium Reactivity of Solids, Gothenburg, 1952, Pt. 1, 373 (Pub. 1954).

3. R.M. Barrer and N. McCallum, J. Chem. Soc., 1953, 4029.

4. R.M. Barrer and E.A.D. White, J. Chem. Soc., 1951, 1267.

5. C. Berger, F.C. Arrance, D.W. Cleaves, and M.J. Plizga, Final Report Contract NAS7-150, March 1964.

6. E.O. Black and T. DeVries, Anal. Chem., 27, 906 (1954).

7. J. O'M. Bockris, G.J. Hills, D. Inman, and L. Young, J. Sci. Inst. 33, 438 (1956).

8. D.W. Breck and N.A. Acara, British Patent 868,846, May 25, 1961.

9. D.W. Breck and N.A. Acara, U.S. Patent 2,950,952, August 30, 1960.

10. D.W. Breck and N.A. Acara, U.S. Patent 2,962,355, November 29, 1960.

11. D.W. Breck and N.A. Acara, U.S. Patent 2,991,151, July 4, 1961.

12. D.W. Breck and N.A. Acara, U.S. Patent 2,995,423, August 8, 1961.

13. D.W. Breck, W.G. Eversole, R.M. Milton, T.B. Reed, and T.L. Thomas, J. Amer. Chem. Soc. 78,5963 (1956).

14. D.W. Breck, E.M. Flanigen, and R.M. Milton, Paper No. 81, 137th ACS Meeting, Cleveland, April 1960.

15. R.L. Broussard and B.P. Shoemaker, J. Amer. Chem. Soc. 82, 1041 (1960).

16. D.C. Freeman, Jr. and D.N. Stamires, J. Chem. Phy. 35, 799 (1961).

17. W.L. Haden, Jr. and F.J. Dzierzanowski, U.S. Patent 2,992,068, July 11, 1961.

18. D.C. Hamby, B.W. Steller, and J.B. Chase, J. Electrochem. Soc. 111, 998 (1964).

19. W.J. Hamer, M.S. Malmberg, and B. Rubin, J. Electrochem. Soc. 103, 8, (1956).

20. P.C. Huang, A. Mizany, and J.L. Pauley, J. Phys. Chem. 68, 2575 (1964).

21. B.W. King, W.A. Hedden, A.B. Tripler,Jr., D.J. Bowers, and B.O. Austin, Ceramic Bul. 43, 117 (1964).

22. R.J. Labrie, J. Electrochem. Soc. 111, 473 (1964).

23. R.J. Labrie and V.A. Lamb, J. Electrochem. Soc. 106, 895 (1959).

24. H.A. Laitinen, et al, Monthly Progress Reports on Contracts DAI-49-186-502-ORD(P)-50; DAI-49-186-502-ORD(P)-187; and DA-11-022-ORD-1987.

25. H.A. Laitinen and B.B. Bhatia, J. Electrochem. Soc. 107, 705 (1960).

26. H.A. Laitinen and C.H. Liu, J. Amer. Chem. Soc. 80, 1015 (1958).

27. H.A. Laitinen and J.W. Pankey, J. Amer. Chem. Soc. 81, 1053 (1959).

28. R.M. Milton, British Patent 841,812, July 20, 1960.

29. R.M. Milton, British Patent 847,057, September 7, 1960.

30. R.M. Milton, British Patent 864,707, April 6, 1961.

31. R.M. Milton, U.S. Patent 2,882,243, April 14, 1959.

32. R.M. Milton, U.S. Patent 2,882,244, April 14, 1959.

33. R.E. Panzer, Electrochem. Tech. 2, 10 (1964).

34. H.E. Rabinowitsch and W.C. Wood, Elektrochem. 39, 562 (1933).

35. S.M. Selis, L.P. McGinnis, E.S. McKee, and J.T. Smith, J. Electrochem. Soc. 110, 469 (1963).

36. S. Senderoff, E.M. Klopp, and M.L. Kronenberg, Progress Report Contract NOrd-18240 AD 277433.

37. Societe D'Etudes, De Recherches et D'Application Pour L'Industrie, Final Report Contract DA-91-591-EUC-2773 OI-360308-D; AD433803, October 31, 1963.

38. D.N. Stamires, J. Chem. Phy., 36, 3174 (1962).

39. D.N. Stamires, et al, Second International Congress on Surface Chemistry, Paris, 1960.

40. E.F. Uhler and G.S. Lozier, Final Report Contract AF33(616)-7505, AD277197, April 1962.

41. Union Carbide Corp. (by R.M. Barrer, P.J. Denny, and E.M. Flanigen), Belgian Patent 615,311; March 22, 1961.

42. Union Carbide Corp. (by D.W. Breck), German Patent 1,098,929, April 14, 1958.

43. Union Carbide Corp. (by D.W. Breck and N.A. Acara), German Patent 1,100,008, September 19, 1957.

44. Union Carbide Corp. (by D.W. Breck and N.A. Acara), German Patent 1,100,009, January 28, 1958.

45. Union Carbide Corp. (by D.W. Breck), German Patent 1,100,010, March 31, 1958.

46. G.F. Zellhoefer, U.S. Patent 3,110,632, November 12, 1963.

47. Philco Research Laboratories, Publication P-24023 (U), February 9, 1964.

48. L.E. Tapol, S.J. Yosim, and R.A. Osteryoung, J. Phys. Chem 65, 1511 (1961).

49. Max Hansen, "Constitution at Binary Alloys," Second Edition, pp. 188-9, McGraw-Hill Book Co., Inc., New York (1958).

50. E.M. Levin, C.R. Robbins, and H.F. McMurdie, "Phase Diagrams for Ceramists," The American Ceramic Society, Columbus, Ohio (1964).

DISTRIBUTION

National Aeronautics and Space Administration
Washington D. C. 20546

Attn: Miss Millie Ruda, Code AFSS-LD — 3 Copies
Walter C. Scott, Code RP — 1 Copy
Ernst M. Cohn, Code RNW — 1 Copy
George F. Esenwein, Code MSA — 1 Copy
A. M. Andrus, Code FC — 1 Copy
J. R. Miles, Code SL — 1 Copy
Welfred M. Redler, Code PE — 1 Copy

National Aeronautics and Space Administration
Goddard Space Flight Center
Greenbelt, Maryland

Attn: Thomas Hennigan, Code 632.2 — 1 Copy
Joseph Shirfey, Code 652 — 1 Copy
Paul Donnelly, Code 636.2 — 1 Copy

National Aeronautics and Space Administration
Lewis Research Center
21000 Brookpark Road
Cleveland, Ohio 44135

Attn: J. D. Sanders, MS 500-201 — 1 Copy

National Aeronautics and Space Administration (Continued)
Lewis Research Center
21000 Brookpark Road
Cleveland, Ohio 44135

Attn: Martin J. Saari, MS 500-201 — 1 Copy
Robert L. Cummings, MS 500-201 — 1 Copy
Harvey J. Schwartz, MS 500-201 — 1 Copy
J. J. Weber, MS 15-1 — 1 Copy
J. E. Dilley, MS 500-309 — 1 Copy
B. Lubarsky, MS 500-201 — 1 Copy
M. R. Unger, MS 500-201 — 1 Copy + 1 repro
Library — 1 Copy

National Aeronautics and Space Administration
Scientific and Technical Information Facility
P. O. Box 5700
Bathesda 14, Maryland

Attn: NASA Representative — 1 Copy

National Aeronautics and Space Administration
Marshall Space Flight Center
Huntsville, Alabama

Attn: Richard Boehme, Bldg 4487-BB, M-ASTR-EC — 1 Copy

National Aeronautics and
Space Administration
Manned Space Craft Center
Houston 1, Texas

Attn: William R. Dusenbury 1 Copy
Propulsion and Energy Systems
Branch
Energy Systems Division
Bldg 16, Site 1

Robert Cohen 1 Copy
Gemini Project Office

National Aeronautics and Space
Administration
Ames Research Center
Pioneer Project
Moffett Field, California

Attn: James R. Swain 1 Copy

Jet Propulsion Laboratory
4800 Oak Grove Drive
Pasadena, California

Attn: Aiji Uchiyama 1 Copy

U. S. Army Engineer Research and
Development Labs
Fort Belvoir, Virginia 22060

Attn: Dr. Galen Frysinger 1 Copy
Electrical Power Branch
SMOFB-EP

U. S. Army Engineer Research and
Development Labs
Fort Monmouth, New Jersey

Attn: David Linden (Code SELRA/PS)
1 Copy

U. S. Army Research and Development
Liaison Group (9851 DV)
APO 757
New York, New York

Attn: B. R. Stein 1 Copy

Army Research Office
Office, Chief Research and Development
Department of the Army
3D 442, The Pentagon
Washington D. C. 20546

Attn: Dr. Sidney J. Magram 1 Copy

Harry Diamond Labs
Room 300, Bldg 92
Connecticut Avenue
and Van Ness Street, N.W.
Washington D. C.

Attn: Nathan Kaplan 1 Copy

Army Materiel Command
Research Division
AMCRD-RSCM T-7
Washington 25, D. C.

Attn: John W. Crellin 1 Copy

U. S. Army TRECOM
Fort Eustis, Virginia 23604

Attn: Dr. R. L. Echols (SMOFE-PSG)
1 Copy

Leonard M. Bartone
(SMOFE-ASE) 1 Copy
Physical Sciences Group
Mechanical Systems Subgroup ASE

U. S. Army Research Office
Box CM, Duke Station
Durham, North Carolina

Attn: Dr. Wilhelm Jorgensen 1 Copy
Paul Greer 1 Copy

U. S. Army Mobility Command
Research Division
Center Line, Michigan 48090

Attn: O. Renius (AMSMO-RR) 1 Copy

Headquarters, U. S. Army Materiel Command
Development Division
Washington 25, D. C.

Attn: Marshall D. Aiken 1 Copy
(AMCRD-DE-MO-P)

Office of Naval Research
Washington D. C. 20360

Attn: Dr. Ralph Roberts, Code 429
Head, Power Branch 1 Copy

Naval Research Laboratory
Washington D. C. 20390

Attn: Dr. J. C. White, Code 6160
1 Copy

Office of Naval Research
Department of the Navy
Washington D. C. 20360

Attn: H. W. Fox, Code 425 1 Copy

Bureau of Naval Weapons
Department of the Navy
Washington 25, D. C.

Attn: Whitwell T. Beatson 1 Copy
(Code RAAE-52)
Milton Knight 1 Copy
(Code RAAE-50)

Bureau of Ships
Department of the Navy
Washington 25, D. C.

Attn: Bernard B. Rosenbaum 1 Copy
(Code 340)

Naval Ordnance Laboratory
Department of the Navy
Corona, California

Attn: Mr. William C. Spindler 1 Copy
(Code 441)

Naval Ordnance Laboratory
Department of the Navy
Silver Spring, Maryland

Attn: Philip B. Cole (Code WB)
1 Copy

Wright-Patterson AFB
Aeronautical Systems Division
Dayton, Ohio

Attn: ASRMFP-2 1 Copy

AF Cambridge Research Lab
L. G. Hanscom Field
Bedford, Massachusetts

Attn: Commander (CRO) 1 Copy

Rome Air Development Center, ESD
Griffiss AFB, New York 13442

Attn: Commander (RAALD) 1 Copy

Headquarters, USAF (AFRDR-AS)
Washington 25, D. C.

Attn: Lt. Col. William G. Alexander
1 Copy

Capt William H. Ritchie
Space Systems Division
Air Force Unit Post Office
Los Angeles 45, California

Attn: SSZAE-11 1 Copy

Capt William Hoover
Air Force Ballistic Missile
Division
Air Force Unit Post Office
Los Angeles 45, California

Attn: WDZYA-21 1 Copy

Mr. Charles F. Yost
Asst Director, Material Sciences
Advanced Research Projects Agency
The Pentagon, Room 3E 153
Washington 25, D. C. 1 Copy

Dr. John H. Huth
Advanced Research Projects Agency
The Pentagon, Room 3E 157
Washington 25, D. C. 1 Copy

U. S. Atomic Energy Commission
Auxiliary Power Branch (SNAP)
Division of Reactor Development
Washington 25, D. C.

Attn: LCOL George H. Ogburn, Jr.
1 Copy

Lt. Col. John H. Anderson
Advanced Space Reactor Branch
Division of Reactor Development
U. S. Atomic Energy Commission
Washington 25, D. C. 1 Copy

Mr. Donald B. Hoatson
Army Reactors, DRD
U. S. Atomic Energy Commission
Washington 25, D. C. 20545 1 Copy

Defense Documentation Center
Headquarters
Cameron Station, Bldg 5
5010 Duke Street
Alexandria 4, Virginia

Attn: TISIA 20 Copies

Office, DDR and E: USW and BSS
The Pentagon
Washington 25, D. C

Attn: G. B. Wareham 1 Copy

Institute for Defense Analyses
Research and Engineering Support Division
1666 Connecticut Avenue, N. W.
Washington 9, D. C.

Attn: Dr. George C. Szego 1 Copy

Power Information Center
University of Pennsylvania
Moore School Building
200 South 33rd Street
Philadelphia 4, Pennsylvania 1 Copy

Office of Technical Services
Department of Commerce
Washington 25, D. C. 20009 1 Copy

Battelle Memorial Institute
505 King Avenue
Columbus 1, Ohio

Attn: Dr. C. L. Faust 1 Copy

Aerojet General Corporation
Chemical Products Division
Azusa, California

Attn: Dr. S. O. Rosenberg 1 Copy

Aeronutronic Division
Philco Corporation
Ford Road
Newport Beach, California

Attn: Dr. S. W. Weller 1 Copy

Allis Chalmers Manaufacturing Company
1100 South 70th Street
Milwaukee 1, Wisconsin

Attn: Dr. Joyner 1 Copy

Arthur D. Little, Incorporated
Cambridge, Massachusetts

Attn: J. H. B. George 1 Copy

Douglas Aircraft Company, Incorporated
Astropower Laboratory
2121 Paularino Avenue
Newport Beach, California

Attn: Dr. Carl Berger 1 Copy

Atomics International Division
North American Aviation, Incorporated
Canoga Park, California

Attn: Dr. H. L. Recht 1 Copy

Electric Storage Battery Company
Carl F. Norberg Research Center
Yardley, Pennsylvania

Attn: W. S. Herbert 1 Copy

Eagle-Picher Company
Post Office Box 290
Joplin, Missouri

Attn: E. M. Morse 1 Copy

Dr. Arthur Fleischer
466 South Center Street
Orange, New Jersey 1 Copy

Electrochimica Corporation
1140 O'Brien Drive
Menlo Park, California

Attn: Dr. Morris Eisenberg 1 Copy

General Electric Corporation
Schenectady, New York

Attn: Dr. William Carson 1 Copy
General Engineering Laboratory

Globe Union, Incorporated
900 East Keefe Avenue
Milwaukee, Wisconsin

Attn: Dr. C. K. Morehouse 1 Copy

Gould-National Batteries, Incorporated
Engineering and Research Center
2630 University Avenue, S. E.
Minneapolis 14, Minnesota

Attn: J. F. Donahue
1 Copy

Gulton Industries
Alkaline Battery Division
Metuchen, New Jersey

Attn: Dr. Robert Shair 1 Copy

Hughes Research Laboratories Corporation
Malibu, California

Attn: T. M. Hahn 1 Copy

Livingston Electronic Corporation
Route 309 opposite Springhouse Quarry
Montgomeryville, Pennsylvania

Attn: William F. Meyers 1 Copy

Lockheed Aircraft Corporation
1123 N. Mathilda Avenue
Sunnyvale, California

Attn: Charles Burell 1 Copy

P. R. Mallory and Company
Northwest Industrial Park
Burlington, Massachusetts

Attn: Dr. Per Bro 1 Copy

Hoffman Electronics Company
Research Laboratory
Santa Barbara, California

Attn: Dr. J. Smatko 1 Copy

Magna Corporation
Division of TRW, Incorporated
101 South East Avenue
Anaheim, California

Attn: Dr. G. Rohrbach
1 Copy

Marquardt Corporation
16555 Saticoy Street
Van Nuys, California

Attn: Dr. H. G. Krull 1 Copy

Melpar, Incorporated
3000 Arlington Boulevard
Falls Church, Virginia

Attn: Dr. R. T. Foley 1 Copy

Midwest Research Institute
425 Volker Boulevard
Kansas City 10, Missouri

Attn: Dr. B. W. Beadle 1 Copy

Monsanto Research Corporation
Everett 49, Massachusetts

Attn: Dr. J. O. Smith 1 Copy

Radio Corporation of America
Somerville, New Jersey

Attn: Dr. H. S. Lozier 1 Copy

Space Technology Laboratories,
Incorporated
2400 E. El Segundo Boulevard
El Segundo, California

Attn: Dr. A. Krausz 1 Copy

Southwest Research Institute
8500 Culebra Road
San Antonio 6, Texas

Attn: Dr. Jan Al
1 Copy

Power Sources Division
Telecomputing Corporation
Laurence Drive
Newbury Park, California

Attn: Dr. M. Shaw 1 Copy

University of Pennsylvania
Electrochemistry Laboratory
Philadelphia 4, Pennsylvania

Attn: Prof. J. O'M. Brockris 1 Copy

Yardney Electric Corporation
New York, New York

Attn: Dr. Paul Howard 1 Copy

Union Carbide Corporation
Parma Research Center
Advanced Developments Department
12900 Snow Road
Parma, Ohio

Attn: Dr. R. A. Charpie 1 Copy

Westinghouse Electric Corporation
Research and Development Center
Churchill Borough
Pittsburgh, Pennsylvania

Attn: Dr. S. Barnartt 1 Copy